Altered gut microbiota activate and expand Insulin B15-23-reactive CD8+ T-cells

Short running title: Gut Microbiota promotes Insulin–Reactive CD8 T Cells

James A. Pearson[1,2], Dimitri Kakabadse[1], Joanne Davies[1], Jian Peng[2], Jeremy Warden-Smith[1], Simone Cuff[1], Mark Lewis[1], Larissa Camargo da Rosa[1], Li Wen[2] and F. Susan Wong[1]

[1]Diabetes Research Group, Institute of Infection and Immunity, School of Medicine, Cardiff University, Cardiff, CF14 4XN, Wales, UK

[2]Section of Endocrinology, School of Medicine, Yale University, New Haven, Connecticut 06519, USA

Correspondence to:
F. Susan Wong
Diabetes Research Group
Institute of Infection and Immunity
School of Medicine
Cardiff University
Cardiff
CF14 4XN
Wales
UK
E-mail: wongfs@cardiff.ac.uk
Telephone: +44 (0)29 2068 7000
ORCID: 0000-0002-2812-8845

Abstract

Insulin is a major autoantigen in type 1 diabetes, targeted by both CD8 and CD4 T-cells. We studied an insulin-reactive T-cell receptor (TCR) alpha-chain transgenic non-obese diabetic (NOD) mouse on a TCRCα and proinsulin2 (PI2)-deficient background, designated as *A22Cα*$^{-/-}$*PI2*$^{-/-}$NOD mice. These mice develop a low incidence of autoimmune diabetes. To test the role of gut microbiota on diabetes development in this model system, we treated the *A22Cα*$^{-/-}$*PI2*$^{-/-}$NOD mice with enrofloxacin, a broad-spectrum antibiotic. The treatment led to male mice developing accelerated diabetes. We found that enrofloxacin increased the frequency of the insulin-reactive CD8+ T-cells and activated the cells in the Peyer's patches (PP) and pancreatic lymph nodes (PLNs), together with induction of immunological effects on the antigen-presenting cell populations. The composition of gut microbiota differed between the enrofloxacin-treated and untreated mice and also between the enrofloxacin-treated mice that developed diabetes, compared with those that remained normoglycemic. Our results provide evidence that the composition of the gut microbiota is important for determining the expansion and activation of insulin-reactive CD8+ T-cells.

Introduction

The incidence of type 1 diabetes (T1D) is increasing worldwide, at a rate too rapid to be associated purely with genetic changes (1), and thus environmental factors, such as the gut microbiota, have been suggested to contribute to T1D development (2). The gut microbiota composition (3-5) and function (6) are altered in patients with T1D. In the Non-obese diabetic (NOD) mouse model, which develops spontaneous autoimmune diabetes similar to humans, altered gut microbiota are also found in the diabetic NOD mice, compared to non-diabetic NOD mice (7). Modifying the gut microbiota by fecal transfer studies (8), dietary changes (9; 10) and the administration of antibiotics (dependent on type, age at which administered and duration) (11-17), all affect diabetes development in NOD mice. Recently, we have shown that islet-specific glucose-6-phosphatase catalytic subunit-related protein-reactive (IGRP) CD8+T-cells can recognize a fusobacterial peptide more strongly than their natural autoantigen (18), suggesting that islet autoimmunity can be activated by molecular mimicry. Furthermore, microbial metabolites released from the diet protect NOD mice by reducing the number of IGRP-reactive CD8+T-cells (10). Interestingly, the development of IGRP-reactive CD8+T-cells is dependent on prior insulin autoimmunity (19; 20).

Proinsulin (PI) is a major autoantigen in humans (21-25) and NOD mice (26-30). Proinsulin is cleaved within the pancreatic beta cells, leading to the regulated secretion of metabolically-active insulin. There are 2 forms of PI in mice, designated PI1 and PI2. PI2 is expressed both in the thymus and pancreas and PI2-deficient mice NOD mice developed accelerated diabetes with 100% penetrance (31), and thus PI2 is considered to be important in the induction of T-cell tolerance.

G9C8 is a highly diabetogenic murine CD8+T-cell clone that recognizes insulin B15-23 through its T-cell receptor (TCR) comprising TCRα chain (*TRAV8-1/TRAJ9*) and TCRβ chain (*TRBV19/TRBJ2-3*) gene rearrangements (32). G9C8 CD8+T-cells can be found in the islets in 4-week-old mice (29), along with other insulin-specific T cells, before islet antigen-specific T-cells of other specificities are detected (33) and are required for the development of other autoantigen-specific CD8+ T-cells (19; 20). We previously generated a transgenic NOD mouse (line 22) with a fixed *TRAV8-1/TRAJ9* TCRα-chain only (29) (termed A22 for simplicity). A22 mice were bred to the PI2-deficient background to study the development and activation of insulin B15-23-reactive CD8+T-cells (34). We found that the PI2-deficient *A22Cα*$^{-/-}$NOD mice had an increased proportion of insulin B15-23-reactive CD8+ T-cells in the pancreatic draining lymph nodes (PLN), compared to *A22Cα*$^{-/-}$NOD mice that have normal levels of PI2. Furthermore, only male, but not female, PI2-deficient *A22Cα*$^{-/-}$NOD mice (*A22Cα*$^{-/-}$*PI2*$^{-/-}$NOD) developed spontaneous diabetes.

In this study, by changing the gut microbiota, we have demonstrated that a broad-spectrum antibiotic enrofloxacin (Baytril) can alter insulin-specific CD8+T-cell function and enable them to expand and become activated, leading to an early onset of diabetes, in *A22Cα*$^{-/-}$*PI2*$^{-/-}$ NOD mice.

Materials and methods

Mice

NOD/Caj mice were originally obtained from Yale University. G9*Cα*$^{-/-}$NOD, G9*Cα*$^{-/-}$*PI2*$^{-/-}$ NOD and *A22Cα*$^{-/-}$*PI2*$^{-/-}$NOD have all been previously described and are summarized in Supplementary Table 1 (34-36). All mice used in the current study were male, from litters divided between treatment groups (Fig.1A). Mice from several breeder pairs were mixed and housed in microisolators or scantainers with food and water *ad libitum,* with 12-hour light and dark cycles in the specific pathogen-free facility at Cardiff University. All procedures were performed in accordance with UK Home Office approved protocols.

Preparation and administration of enrofloxacin-treated water

Enrofloxacin (Bayer) was added to autoclaved, filtered water at a final concentration of 0.4mg/ml (diluted 1:250), prepared freshly every week. Untreated mice received the same autoclaved, filtered water. Mice were treated from 3-weeks of age (at weaning) continuously until 10-weeks of age, unless otherwise stated.

Diabetes Incidence

Mice were monitored weekly for glycosuria (Bayer Diastix) from 5-weeks of age until termination. Diabetes was diagnosed after 2 consecutive positive glycosuria tests, confirmed by a blood glucose concentration >13.9mmol/L (>250mg/dl). Statistical analysis was performed using the log-rank test.

Surface and Intracellular staining

Lymphoid tissues including spleen, pancreatic lymph nodes (PLN), mesenteric lymph nodes (MLN) and Peyer's patches (PP) were collected from 6-week-old or 10-week-old mice. Cells were homogenized and filtered. Splenic red blood cells were lysed using water, followed by 10xPBS. $1x10^6$ cells were then incubated with TruStain FcX (BioLegend) in PBS+0.5% BSA at 4°C for 10min prior to cell staining (4°C, 30min) using combinations of the following monoclonal antibodies (all from BioLegend unless stated): anti-B220, anti-CD4, anti-CD8α, anti-CD11b, anti-CD11c, anti-CD19, anti-CD80, anti-CD103, anti-F4/80, anti-TCRbeta, anti-TCRVbeta4, anti-TCRVbeta5.1-5.2, anti-TCRVbeta6, anti-TCRVbeta8.1-8.2 (BD), anti-TCRVbeta12 (eBioscience), anti-TCRVbeta11 (eBioscience), anti-TCRVbeta14 (BD) and anti-MHCII (BD) in the presence of a viability dye (BioLegend or eBioscience).

For Intracellular cell staining, $1-2x10^6$ cells were incubated at 37°C in the presence of 50ng/ml PMA, 500ng/ml Ionomycin and 2μM Monensin (all from Sigma-Aldrich) for 4hours. Cells were then stained for surface molecules prior to fixation/permeabilization and the addition of intracellular monoclonal antibodies (all BioLegend): anti-IFN-gamma, anti-IL-10 or anti-FoxP3. Cells were analyzed on a BD LSRFortessa FACS machine and subsequently analyzed with FlowJo software version 8.8.6. Statistical analysis was performed by Student's t test.

Generating Tetramers

H-$2K^d$-LYLVCGERG monomers or H-$2K^d$-AYAAAAAAV monomers (National Institutes of Health Tetramer Core Facility) were slowly defrosted on ice. Tetramers were made as described previously (37).

Tetramer Staining

Tetramer staining was conducted as previously reported (34). G9C8 transgenic T-cells (35) or NY8.3 transgenic T-cells (38) were used as a positive control. The minimal H-2K^{d}-AYAAAAAAV tetramer was used to determine non-specific background, which was then subtracted from the H-2K^{d}-LYLVCGERG-Brilliant Violet 421 or H-2K^{d}-VYLKTNVFL-Allophycocyanin tetramer staining result respectively. Cells were analyzed as above. Statistical analysis was performed by Student's t test.

Fecal bacterial extraction

Fecal samples from 3-week and 6-week-old mice were collected. Fecal bacteria were extracted and sequenced as previously described (8). β-Diversity was calculated to compare differences between microbial community profiles, and the data are shown as a principal coordinate analysis (PCoA). Microbial composition was analyzed by Student's t test with β-Diversity PCoA plots analyzed by ANOSIM.

In vitro **antigen presentation**

CD11c+ and CD11b+ cells were isolated from the spleens of 6-week-old *A22Cα*$^{-/-}$*PI2*$^{-/-}$NOD mice untreated or treated with enrofloxacin. CD8+T-cells were isolated by negative selection from the spleen of 6-week-old G9*Cα*$^{-/-}$NOD mice. All cell isolations were conducted following the manufacturer's protocols (Miltenyi). CD8+T-cells were CFSE-labeled and co-cultured with the antigen-presenting cells (APCs) in a 1:1 ratio, for 48 hours, in the presence

or absence of insulin B15-23 peptide. Cells were stained for surface markers and analyzed as previously described. Statistical analysis was performed by Student's t test.

In vitro splenocyte:bacteria co-culture

The small intestine was harvested from 6-week-old mice and flushed with 5mls sterile PBS. The gut contents were mixed thoroughly by vortex for 2mins, followed by centrifuging for 5mins at low speed (52xg) to remove dietary residue. The supernatant was transferred to a new tube and spun. After washing the pellet twice more, the combined supernatant was centrifuged at 469xg to remove mammalian cells. Bacteria in the supernatant were pelleted by high-speed centrifugation (1876xg, 5mins) and resuspended in PBS. Bacterial concentration was measured with a spectrophotometer (Bio-Rad) and heat-inactivated at 90°C for 20mins. 10^8 heat-inactivated bacteria were co-cultured with splenocytes ($2x10^6$/ml) for 12hours prior to the addition of 50ng/ml PMA, 500ng/ml Ionomycin in the presence of 2μM Monensin (all Sigma-Aldrich). 4hours later, cells were then stained for surface and intracellular markers as outlined above. Statistical analysis was performed by multiple Student's t tests, corrected using FDR.

Results

Enrofloxacin treatment accelerates and increases spontaneous diabetes development in male PI2-deficient TRAV8-1/TRAJ9Cα$^{-/-}$ NOD mice

Single TCRα chain transgenic NOD mice, utilizing the TCR *TRAV8-1/TRAJ9Cα$^{-/-}$* (designated *A22Cα$^{-/-}$*) (34), bred with PI2-deficient mice (*A22Cα$^{-/-}$PI2$^{-/-}$),* have elevated levels

of insulin B15-23-reactive CD8+T-cells and develop a low incidence of spontaneous diabetes. To test whether the gut microbiota may influence the expansion and activation of insulin B15-23-reactive CD8+T-cells, as recently reported for other autoreactive T-cells (18; 39; 40), we administered enrofloxacin (a broad-spectrum antibiotic), to either the breeder *A22Cα$^{-/-}$PI2$^{-/-}$*NOD mice throughout pregnancy, or to the *A22Cα$^{-/-}$PI2$^{-/-}$*NOD pups from weaning at 3 weeks (Fig.1A). We found that spontaneous diabetes developed in ~50% of *A22Cα$^{-/-}$PI2$^{-/-}$*NOD male mice given enrofloxacin at the time of weaning, compared to *A22Cα$^{-/-}$PI2$^{-/-}$*NOD mice never exposed to enrofloxacin (~10%), or to *A22Cα$^{-/-}$PI2$^{-/-}$*NOD mice treated with enrofloxacin from birth (15%), or from birth to weaning only (0%) (Fig.1B). We repeated this experiment focusing only on mice given enrofloxacin from weaning (enrofloxacin-treated), compared to untreated mice and again found a significant increase in spontaneous diabetes development in those given enrofloxacin from weaning (Fig.1C). Whereas the *A22Cα$^{-/-}$PI2$^{-/-}$*NOD mice have the same TCRα chain as G9C8 CD8+T-cells but can pair with any endogenous TCRβ chain, the G9*Cα$^{-/-}$PI2$^{-/-}$*NOD mice express both the rearranged G9C8TCRα and β chains. Interestingly, unlike the effect in *A22Cα$^{-/-}$PI2$^{-/-}$*NOD mice, enrofloxacin did not affect the incidence of diabetes in G9*Cα$^{-/-}$PI2$^{-/-}$* NOD mice (Fig.1D). Thus, gut bacterial composition may alter expansion of particular TCR clonotypes, other than the clonotypic G9C8TCR, that recognize insulin B15-23, which we next investigated.

Enrofloxacin treatment leads to Insulin B15-23-reactive CD8+T-cell expansion, altered TRBV repertoire and activation

All T-cells in *A22Cα*$^{-/-}$*PI2*$^{-/-}$NOD mice have the fixed TCRα chain derived originally from a CD8+T-cell and thus, we investigated the effect of enrofloxacin treatment on shaping the CD8+T-cell compartment. We found that in all tissues, except the Peyer's patches (PP), there was an age-associated increase in CD8+T-cells, while CD4+T-cells were reduced (Supplementary Fig.1A-B and (34)). No significant differences in the proportion of FoxP3+Tregs between enrofloxacin-treated or untreated mice were observed in the PLN (Supplementary Fig.1C) or PP, although there was an age-related increase in the untreated mice.

To identify the insulin-specific CD8+T-cells, we used an insulin B15-23-tetramer to investigate if antibiotic usage affected insulin B15-23-specific CD8+T-cells in different lymphoid tissues. Interestingly, our results demonstrated a significant increase in the proportion and number of insulin B15-23-tetramer-positive CD8+T-cells in the PLN, MLN and PP of both 6-week-old and 10-week-old *A22Cα*$^{-/-}$*PI2*$^{-/-}$NOD mice treated with enrofloxacin compared to the untreated mice (Fig.2A-B and Supplementary Fig.2A). The expansion of these insulin-reactive CD8+T-cells was more pronounced in the 6-week-old mice, corresponding with the earliest development of diabetes in the enrofloxacin-treated mice. Moreover, we observed an increased percentage of activated (CD69+) tetramer-positive CD8+T-cells in the PLN and PP of 6-week-old and 10-week-old enrofloxacin-treated mice respectively, compared to the untreated mice (Fig.2C-D and Supplementary Fig.2B). We also observed that tetramer-negative CD8+CD69+T-cells were reduced in the PP with age in untreated mice, while they remained at a consistent proportion in enrofloxacin-treated mice (Supplementary Fig.2C-D). Furthermore, we found that, in both

the PLN and PP of enrofloxacin-treated mice, the effector/memory (CD44+CD62L-) population of Insulin B15-23-tetramer-positive CD8+T-cells significantly increased with age (Fig.2E-F and Supplementary Fig.2E). The opposite trend was observed in untreated mice. Interestingly, in tetramer-negative CD8+T-cells we observed an increased effector/memory population only at 10-weeks of age in enrofloxacin-treated mice vs untreated mice (Supplementary Fig. 2F-G). We further analyzed TCRVβ usage and found changes in multiple TCRVβ chains in both the total CD8+T-cell repertoire and the insulin-specific CD8+T-cell repertoire from the PLN and PP (Fig.2G-H and Supplementary Fig.3-4). Interestingly, no significant differences were observed in the selection of TCRVβ6 (the chain used by G9C8 T-cells). These data indicate earlier activation of the insulin-reactive CD8+T-cells in the PLN of enrofloxacin-treated mice, as well as more highly activated insulin-reactive CD8+T-cells, which have an altered TCRβ repertoire, in the PP of 10-week-old mice.

Enrofloxacin alters antigen-presenting cells (APCs)

To explore the mechanism by which enrofloxacin treatment led to the increase in activated insulin-B15-23-specific CD8+T-cells in *A22Cα*$^{-/-}$*PI2*$^{-/-}$NOD mice, we tested antigen-presenting cells (APC) from the PLN and PP. Here, we found changes in dendritic cells (DC) and macrophages (Fig.3A-F and Supplementary Fig.5), as was observed in other studies using antibiotics in wild-type NOD mice (14; 16). CD103 is an integrin marker of migratory DCs (41), and influenced by microbial challenge (42). We found a reduction in both CD11c+CD103+ and CD11b+CD103+cells in the PP of the enrofloxacin-treated mice at 6

weeks, compared to untreated mice but an increase at 10 weeks, whereas in untreated mice, these cells were reduced with age (Fig.3A-B). These effects were not observed in the PLN (data not shown). Moreover, the DCs and macrophages expressed increased IFN-gamma production, particularly in 6-week-old enrofloxacin-treated mice (Fig.3C-D). There were also fewer IL-10-producing DCs, with a similar trend in the macrophages in the enrofloxacin-treated mice, compared to control mice at 6 weeks (Fig.3E-F), although not sustained by 10 weeks. Although it has been suggested that CD11b+CD11c+cells are more inflammatory (43), we did not find any changes in CD11b+CD11c+cells nor in B-cells in the PP, including IgA+B-cells (Supplementary Fig.6).

To determine whether these APC subsets were able to promote the proliferation of insulin-reactive CD8+T-cells, CFSE-labeled G9C8 CD8+T-cells were co-cultured with CD11c+cells or CD11b+cells from donors treated with or without enrofloxacin in the presence of insulin B15-23 peptide. We found CD11c+cells but not CD11b+cells, from enrofloxacin-treated mice promoted the proliferation of insulin-reactive CD8+T-cells (Fig.3G-H and Supplementary Fig.7). This was not due to a direct action of enrofloxacin on the cells as we tested the effect of enrofloxacin in cell culture and this decreased CD69 expression in T-cells at lower peptide concentrations compared to the effects seen in the absence of enrofloxacin but no differences were found in IFN-gamma secretion (Supplementary Fig.8), suggesting that the enrofloxacin treatment affected the APCs in the enrofloxacin-treated mice, and these played an important role in modifying T-cell function. Thus enrofloxacin treatment induced a more inflammatory profile in some APC subsets, which could contribute to increased activation of insulin-reactive CD8+T-cells, particularly at 6 weeks of age.

Enrofloxacin modifies the gut microbiota

Enrofloxacin targets both gram-positive and gram-negative bacteria and therefore, we asked whether altered microbiota were driving diabetes development. We sequenced gut microbiota from the fecal pellets of 3-week-old mice (pre-antibiotic treatment) and 6-week-old mice (3 weeks after commencement of antibiotics) when most diabetes develops. Interestingly, α-diversity (referring to total bacterial diversity), as measured by Chao richness, was not altered in the enrofloxacin-treatment groups, regardless of diabetes development and age (Supplementary Fig.9A). Furthermore, no significant differences in β-diversity (differences in the bacterial composition between treated and untreated mice) were seen at 3 weeks of age, confirming that there was no initial pre-treatment difference in bacterial composition that could contribute to altered diabetes development (Supplementary Fig.9B). However, we observed significant differences in 6-week-old enrofloxacin-treated compared with untreated mice (Fig.4A). Further, enrofloxacin-treated mice had a decrease in the relative abundance of *Allobaculum*, *Turicibacter* and *Bifidobacterium*, but increased abundances of *Coprococcus* and *Oscillospira* (all at the genus level) compared to untreated mice (Fig.4B). *Bifidobacterium* has been associated with reducing gut permeability (44) and *Oscillospira* is associated with increased gut permeability (45). Thus, the reduced *Bifidobacterium* and increased *Oscillospira* induced by enrofloxacin may both promote a more permeable intestinal epithelial barrier in our mice. Next, we compared the composition of gut microbiota in enrofloxacin-treated *A22Cα*$^{-/-}$*PI2*$^{-/-}$NOD mice, which did not develop diabetes, to those that later developed disease. Although there were no significant

differences in β-diversity in 6-week-old enrofloxacin-treated mice, with or without diabetes, some of the samples from the diabetic mice clustered closely, whereas the others were scattered widely (Fig.4C). However, there were significant differences at the genus, family and species level between these two groups (Fig.4D). These included increased relative abundances of *Adlercreutzia* (genus level), *Roseburia* (genus level), *Lachnospiraceae* (family level) and *Bacteroidetes ovatus* (species level) in those mice that later developed diabetes, compared to those that were protected (Fig.4D). Our results are in line with the findings by Krych and colleagues, who demonstrated an increased relative abundance of *Firmicutes* (inclusive of *Coprococcus*, *Oscillospira*, *Lachnospiraceae* and *Roseburia*), correlated to diabetes development in wild-type NOD mice (7).

Enrofloxacin-modified gut microbiota promote stronger proinflammatory immune responses

To assess the functional effects of the microbiota induced by enrofloxacin treatment and diabetes development, we performed crisscross *in vitro* cultures of splenocytes from 6- and 10-week-old mice, with heat-killed microbiota from enrofloxacin-treated diabetic and non-diabetic mice, as well as from untreated non-diabetic mice (all microbiota donors were 6 weeks old), as controls. We also cultured splenocytes from each of the mouse groups, without gut bacteria, and no differences were found between any of the groups.

Gut bacteria from the diabetic enrofloxacin-treated donors induced the highest proportion of IFN-gamma-producing CD8+T-cells in the splenocytes of 6- and 10-week-old untreated mice compared to the gut bacteria from non-diabetic enrofloxacin-treated and untreated mice (Fig.5A-B and Supplementary Fig.10). Furthermore, gut bacteria from enrofloxacin-treated

donors, with or without diabetes, induced a greater frequency of IFN-gamma-producing splenocyte CD11b+cells from enrofloxacin-treated mice compared to splenocyte CD11b+cells from untreated mice (Fig.5C and Supplementary Fig.11). It is interesting that the profile was reversed by 10 weeks of age, with the highest frequency of IFN-gamma-producing splenocyte CD11b+cells of untreated mice, following culture with bacteria (Fig.5D). We found no significant differences in the induction of IFN-gamma-producing splenocyte CD11c+cells of 6- or 10-week-old mice, by the different sources of bacteria (Fig.5E-F and Supplementary Fig.12). Splenocyte CD11b+cells from 6-week old treated and 10-week-old untreated mice showed the strongest inflammatory response to the gut bacteria, regardless of the source (Fig.5C-D). We found no obvious changes in TGF-beta-, IL-10-, IL-17a-, IL-12/23- and TNF-alpha-producing CD11b+CD11c+cells, B-cells or CD4+T-cells (data not shown). Finally, we tested the inflammatory response of splenocytes from *G9Cα*$^{-/-}$ NOD mice (expressing the G9C8TCR) to gut microbiota from enrofloxacin-treated and non-treated mice. Our results confirmed that the microbiota from enrofloxacin-treated mice were more proinflammatory, as significantly higher numbers of IFN-gamma-producing G9C8 CD8+T-cells were found in response to the gut bacteria from enrofloxacin-treated mice compared to the G9C8 CD8+T-cells cultured with the microbiota from untreated mice (Fig.6A and Supplementary Fig.13A). We also observed enhanced IFN-gamma-producing splenocyte CD11b+cells in response to microbiota from diabetic enrofloxacin-treated mice compared to bacteria from untreated mice (Fig.6B and Supplementary Fig.13B), with a similar trend in splenocyte CD11c+cells (Fig.6C and Supplementary Fig.13C). Together our

data demonstrate that enrofloxacin treatment of *A22Cα$^{-/-}$PI2$^{-/-}$*NOD mice promotes more IFN-gamma-inducing gut microbiota.

Enrofloxacin treatment of NOD mice leads to Insulin B15-23-reactive CD8+T-cell expansion and activation within the Peyer's Patches

To assess the effect of enrofloxacin treatment on insulin B15-23-reactive CD8+T-cells in a non-TCR restricted mouse, we treated male NOD mice with/without enrofloxacin from weaning for 3 weeks. We found enrofloxacin treatment significantly altered the gut microbiota composition after 3 weeks of treatment (Fig.7A-B). However, the microbiota changes induced by enrofloxacin treatment were different in the NOD mice, compared to the *A22C α$^{-/-}$PI2$^{-/-}$*NOD mice (Fig.4) likely due to the TCR-restriction contributing to altered microbiota composition (Supplementary Fig.14). We demonstrated that enrofloxacin treatment expanded the number of insulin B15-23-reactive CD8+T-cells within the PP (Fig. 7C and Supplementary Fig.15A-B), with a trend to an increase in proportion. In addition, we also observed an increase in the MFI of the tetramer staining in the PLN of enrofloxacin-treated mice compared to untreated mice (Supplementary Fig.15C). The number and proportion of CD69-expressing insulin-reactive CD8+T-cells was also higher in the PLN and PP of enrofloxacin-treated NOD mice (Fig.7D and Supplementary Fig.15D-E). However, these enrofloxacin-induced changes were restricted to the insulin B15-23-reactive CD8+T-cells, as we found no significant differences in the proportion, number or activation of the IGRP-reactive CD8+T-cells (Supplementary Fig.16). We also observed increased IFN-gamma secretion by CD8+T-cells, CD11c+cells and CD11b+cells in enrofloxacin-treated NOD mice compared to untreated mice in all tissues (Fig.7E-G and Supplementary Fig.17). Thus, our data suggests

enrofloxacin treatment can promote the expansion and activation of insulin B15-23-reactive CD8+T-cells and IFN-gamma secretion in both TCR α -restricted and non-TCR restricted NOD mice.

Discussion

In this study we investigated how changing the gut microbiota, using a broad-spectrum antibiotic (Enrofloxacin), influenced the TCRβ repertoire, together with expansion and activation of insulin-reactive CD8+T-cells, thereby leading to a higher incidence of diabetes. Our study has demonstrated that the altered gut microbiota induced a strong IFN-gamma response from a number of cell types, particularly, the CD8+T-cells.

Using a mouse model with a restricted insulin-reactive TCRα chain but polyclonal TCRβ chains (both insulin-reactive and non-insulin reactive), we found alterations in the TCRβ repertoire influenced by gut microbiota, not previously been reported in any diabetes-related microbiome studies. It is known that the Treg TCR repertoire can be strongly influenced by the gut microbiota composition, arising from tolerogenic antigen presentation and conversion of T-cells into Tregs (46-48). Our current study demonstrates that the TCR repertoire can clearly be influenced by altering gut microbiota through antibiotic usage, which in turn affects the development of diabetes. These changes in TCR repertoire likely arise due to expansions of CD8+T-cells recognizing the altered microbiota composition. Interestingly, enrofloxacin administration to G9C8TCRαβ mice, in which both G9TCRα and TCRβ were fixed, did not alter the incidence of diabetes. This suggests that the altered diabetes incidence we observed in this study was related to the increased expansion of cells with different TCRβ chains. It

also emphasizes the importance of the effect that environmental factors, such as the microbiota, may have on different T-cell clonotypes. Not only is T-cell selection affected by the different gut microbial composition, but the antigen-specific T-cells also are more activated and expand to increase diabetes incidence.

As other studies have shown, antibiotic treatment can influence the composition of gut microbiota (11-17). While most of these studies investigated female NOD mice, one study has focused on the male NOD mice that developed diabetes (17). It has been shown that hormones can influence the gut microbiota and contribute to diabetes susceptibility in NOD mice (49; 50). Interestingly, we have previously shown that, in our model system, female *A22Cα*$^{-/-}$*PI2*$^{-/-}$NOD did not develop T1D (34). Therefore, our current study was focused on male *A22Cα*$^{-/-}$*PI2*$^{-/-}$NOD mice. It is conceivable that the microbiota in our *A22Cα*$^{-/-}$*PI2*$^{-/-}$NOD mice may also be influenced by sex hormones, and thus contribute to the dichotomy of diabetes development in the different sexes.

A recent study showed that IGRP-reactive CD8+T-cells can recognize a microbial mimic (18; 40); it is possible that insulin-reactive CD8+T-cells may also do so, as the human insulin-reactive 1E6 clone can recognize a bacterial peptide from a common human pathogen (25). However, it is unknown whether the bacteria themselves can stimulate this T-cell clone *in vivo*. Thus to date, no bacterial mimics for insulin have yet been identified that can alter diabetes development. Given the ability of autoreactive CD8+T-cells to recognize a vast number of peptides (51), it is highly likely, there will be some insulin mimics. It is also possible that the changes in the composition of gut microbiota, especially *Bifidobacteria* and *Oscillospira,* altered gut permeability in our mice. *Bifidobacterium* can reduce gut

permeability (44) while *Oscillospira* is associated with increasing gut permeability (45). Although it is not currently clear which specific bacteria played the dominant role in our study, we present evidence that the microbiota clearly affected insulin-reactive T-cell development, activation, expansion and function, particularly in relation to IFN-gamma secretion, leading to increased incidence of diabetes.

Our investigation of other subsets of immune cells revealed relatively small changes in non-CD8+T-cells. However, we found changes in macrophages and DCs within the PP and PLN linked to CD103 expression, as well as altered IFN-gamma and IL-10 secretion. Furthermore, upon bacterial stimulation, the macrophages and DCs exhibited enhanced IFN-gamma secretion. Our data suggest a direct effect of the altered composition of microbiota on immune cells to secrete proinflammatory cytokines. It is interesting that age-related differences were observed between treatment groups e.g. enrofloxacin-treated CD11b+cells from 6-week old mice exposed to microbiota produced more IFN-gamma compared to untreated mice. However, at 10 weeks of age, this trend was reversed. These time-dependent effects may arise from changes to immune cell:microbiota interactions *in vivo,* and this may include effects from microbial changes associated with aging as well as changes to gut permeability. Furthermore, we have also demonstrated that CD11c+cells from enrofloxacin-treated mice can promote insulin-specific CD8+T-cell proliferation *in vitro* compared to cells from untreated donors.

In conclusion, we suggest that insulin-reactive pathogenic CD8+T-cells can be activated and expanded by altered gut bacteria as a result of antibiotic treatment. The altered gut microbiota also promote inflammatory APCs, which in turn facilitate the expansion and activation of a

number of different clonotypes of insulin-reactive CD8+T-cells, leading to the development of accelerated autoimmune diabetes, in our NOD transgenic mouse model of autoimmune diabetes. We also confirmed similar effects in non-TCR transgenic NOD mice, in which we observed that enrofloxacin treatment promoted the expansion and activation of insulin-reactive CD8+T-cells, as well as promoting IFN-gamma secretion. Our study provides evidence that the gut microbiota play an important role in activating the insulin-specific autoimmune response early in life, which then later affects diabetes development.

Acknowledgements

The authors thank the National Institutes of Health Tetramer Core Facility for provision of the H-2K^{d}-LYLVCGERG tetramer and minimal binding tetramers H-2K^{d}- AYAAAAAAV. We thank Karl Hager (Lab Medicine, Yale School of Medicine, Yale University) for assistance with 16S rRNA sequencing.

Funding

JAP was a recipient of a Diabetes UK PhD studentship and subsequently a Fulbright-Diabetes UK postdoctoral research scholarship. The work was funded by an EFSD grant (NN 2014_6) and MRC grant (G0901155) to FSW; NIH grants (DK092882, DK100500, and P30 DK945735) to LW.

Duality of interest

No potential conflicts of interest relevant to this article were reported.

Author Contributions

J.A.P., L.W. and F.S.W. designed the experiments; J.A.P., D.K., J.D., J.P., J.W.S., S.T., M.L. and L.C.D.R. performed the experiments; J.A.P., L.W. and F.S.W. analyzed the results and wrote the manuscript. L.W. and F.S.W. supervised the study; the project was conceived by F.S.W. F.S.W. is the guarantor of this work and, as such, had full access to all the data in the study and takes responsibility for the integrity of the data and the accuracy of the data analysis.

Prior Presentation

Parts of this study were presented in abstract form as poster presentations at the Immunology of Diabetes Society Congress 2018, London, U.K., 25–29 October 2018, and at the Keystone Symposia on Molecular and Cellular Biology: Gut Microbiota Modulation of Host Physiology: The Search for Mechanism, Keystone, CO, 1–6 March 2015.

References

1. Gillespie KM, Bain SC, Barnett AH, Bingley PJ, Christie MR, Gill GV, Gale EAM: The rising incidence of childhood type 1 diabetes and reduced contribution of high-risk HLA haplotypes. Lancet 2004;364:1699-1700
2. Wong FS, Hu C, Zhang L, Du W, Alexopoulou L, Flavell RA, Wen L: The role of Toll-like receptors 3 and 9 in the development of autoimmune diabetes in NOD mice. Ann N Y Acad Sci 2008;1150:146-148
3. de Goffau MC, Luopajärvi K, Knip M, Ilonen J, Ruohtula T, Härkönen T, Orivuori L, Hakala S, Welling GW, Harmsen HJ, Vaarala O: Fecal microbiota composition differs between children with β-cell autoimmunity and those without. Diabetes 2013;62:1238-1244
4. de Goffau MC, Fuentes S, van den Bogert B, Honkanen H, de Vos WM, Welling GW, Hyoty H, Harmsen HJ: Aberrant gut microbiota composition at the onset of type 1 diabetes in young children. Diabetologia 2014;57:1569-1577

5. Kostic AD, Gevers D, Siljander H, Vatanen T, Hyötyläinen T, Hämäläinen AM, Peet A, Tillmann V, Pöhö P, Mattila I, Lähdesmäki H, Franzosa EA, Vaarala O, de Goffau M, Harmsen H, Ilonen J, Virtanen SM, Clish CB, Orešič M, Huttenhower C, Knip M, Xavier RJ, Group DS: The dynamics of the human infant gut microbiome in development and in progression toward type 1 diabetes. Cell Host Microbe 2015;17:260-273
6. Vatanen T, Kostic AD, d'Hennezel E, Siljander H, Franzosa EA, Yassour M, Kolde R, Vlamakis H, Arthur TD, Hämäläinen AM, Peet A, Tillmann V, Uibo R, Mokurov S, Dorshakova N, Ilonen J, Virtanen SM, Szabo SJ, Porter JA, Lähdesmäki H, Huttenhower C, Gevers D, Cullen TW, Knip M, Xavier RJ, Group DS: Variation in Microbiome LPS Immunogenicity Contributes to Autoimmunity in Humans. Cell 2016;165:842-853
7. Krych Ł, Nielsen DS, Hansen AK, Hansen CH: Gut microbial markers are associated with diabetes onset, regulatory imbalance, and IFN-γ level in NOD mice. Gut Microbes 2015;6:101-109
8. Peng J, Narasimhan S, Marchesi JR, Benson A, Wong FS, Wen L: Long term effect of gut microbiota transfer on diabetes development. J Autoimmun 2014;53:85-94
9. Marietta EV, Gomez AM, Yeoman C, Tilahun AY, Clark CR, Luckey DH, Murray JA, White BA, Kudva YC, Rajagopalan G: Low incidence of spontaneous type 1 diabetes in non-obese diabetic mice raised on gluten-free diets is associated with changes in the intestinal microbiome. PLoS One 2013;8:e78687
10. Mariño E, Richards JL, McLeod KH, Stanley D, Yap YA, Knight J, McKenzie C, Kranich J, Oliveira AC, Rossello FJ, Krishnamurthy B, Nefzger CM, Macia L, Thorburn A, Baxter AG, Morahan G, Wong LH, Polo JM, Moore RJ, Lockett TJ, Clarke JM, Topping DL, Harrison LC, Mackay CR: Gut microbial metabolites limit the frequency of autoimmune T cells and protect against type 1 diabetes. Nat Immunol 2017;18:552-562
11. Hansen CH, Krych L, Nielsen DS, Vogensen FK, Hansen LH, Sørensen SJ, Buschard K, Hansen AK: Early life treatment with vancomycin propagates Akkermansia muciniphila and reduces diabetes incidence in the NOD mouse. Diabetologia 2012;55:2285-2294
12. Tormo-Badia N, Håkansson A, Vasudevan K, Molin G, Ahrné S, Cilio CM: Antibiotic treatment of pregnant non-obese diabetic (NOD) mice leads to altered gut microbiota and intestinal immunological changes in the offspring. Scand J Immunol 2014; 80:250–260
13. Candon S, Perez-Arroyo A, Marquet C, Valette F, Foray AP, Pelletier B, Milani C, Ventura M, Bach JF, Chatenoud L: Antibiotics in early life alter the gut microbiome and increase disease incidence in a spontaneous mouse model of autoimmune insulin-dependent diabetes. PLoS One 2015;10:e0125448
14. Hu Y, Peng J, Tai N, Hu C, Zhang X, Wong FS, Wen L: Maternal Antibiotic Treatment Protects Offspring from Diabetes Development in Nonobese Diabetic Mice by Generation of Tolerogenic APCs. J Immunol 2015;195:4176-4184
15. Nobel YR, Cox LM, Kirigin FF, Bokulich NA, Yamanishi S, Teitler I, Chung J, Sohn J, Barber CM, Goldfarb DS, Raju K, Abubucker S, Zhou Y, Ruiz VE, Li H, Mitreva M, Alekseyenko AV, Weinstock GM, Sodergren E, Blaser MJ: Metabolic and metagenomic outcomes from early-life pulsed antibiotic treatment. Nat Commun 2015;6:7486

16. Hu Y, Jin P, Peng J, Zhang X, Wong FS, Wen L: Different immunological responses to early-life antibiotic exposure affecting autoimmune diabetes development in NOD mice. J Autoimmun 2016;72:47-56
17. Livanos AE, Greiner TU, Vangay P, Pathmasiri W, Stewart D, McRitchie S, Li H, Chung J, Sohn J, Kim S, Gao Z, Barber C, Kim J, Ng S, Rogers AB, Sumner S, Zhang XS, Cadwell K, Knights D, Alekseyenko A, Bäckhed F, Blaser MJ: Antibiotic-mediated gut microbiome perturbation accelerates development of type 1 diabetes in mice. Nat Microbiol 2016;1:16140
18. Tai N, Peng J, Liu F, Gulden E, Hu Y, Zhang X, Chen L, Wong FS, Wen L: Microbial antigen mimics activate diabetogenic CD8 T cells in NOD mice. J Exp Med 2016;213:2129-2146
19. Krishnamurthy B, Dudek NL, McKenzie MD, Purcell AW, Brooks AG, Gellert S, Colman PG, Harrison LC, Lew AM, Thomas HE, Kay TW: Responses against islet antigens in NOD mice are prevented by tolerance to proinsulin but not IGRP. J Clin Invest 2006;116:3258-3265
20. Krishnamurthy B, Mariana L, Gellert SA, Colman PG, Harrison LC, Lew AM, Santamaria P, Thomas HE, Kay TW: Autoimmunity to both proinsulin and IGRP is required for diabetes in nonobese diabetic 8.3 TCR transgenic mice. J Immunol 2008;180:4458-4464
21. Schloot NC, Willemen S, Duinkerken G, de Vries RR, Roep BO: Cloned T cells from a recent onset IDDM patient reactive with insulin B-chain. J Autoimmun 1998;11:169-175
22. Semana G, Gausling R, Jackson RA, Hafler DA: T cell autoreactivity to proinsulin epitopes in diabetic patients and healthy subjects. J Autoimmun 1999;12:259-267
23. Skowera A, Ellis RJ, Varela-Calviño R, Arif S, Huang GC, Van-Krinks C, Zaremba A, Rackham C, Allen JS, Tree TI, Zhao M, Dayan CM, Sewell AK, Unger WW, Unger W, Drijfhout JW, Ossendorp F, Roep BO, Peakman M: CTLs are targeted to kill beta cells in patients with type 1 diabetes through recognition of a glucose-regulated preproinsulin epitope. J Clin Invest 2008;118:3390-3402
24. Bulek AM, Cole DK, Skowera A, Dolton G, Gras S, Madura F, Fuller A, Miles JJ, Gostick E, Price DA, Drijfhout JW, Knight RR, Huang GC, Lissin N, Molloy PE, Wooldridge L, Jakobsen BK, Rossjohn J, Peakman M, Rizkallah PJ, Sewell AK: Structural basis for the killing of human beta cells by CD8(+) T cells in type 1 diabetes. Nat Immunol 2012;13:283-289
25. Cole DK, Bulek AM, Dolton G, Schauenberg AJ, Szomolay B, Rittase W, Trimby A, Jothikumar P, Fuller A, Skowera A, Rossjohn J, Zhu C, Miles JJ, Peakman M, Wooldridge L, Rizkallah PJ, Sewell AK: Hotspot autoimmune T cell receptor binding underlies pathogen and insulin peptide cross-reactivity. J Clin Invest 2016;126:3626
26. Wegmann DR, Norbury-Glaser M, Daniel D: Insulin-specific T cells are a predominant component of islet infiltrates in pre-diabetic NOD mice. Eur J Immunol 1994;24:1853-1857
27. Wegmann DR, Gill RG, Norbury-Glaser M, Schloot N, Daniel D: Analysis of the spontaneous T cell response to insulin in NOD mice. J Autoimmun 1994;7:833-843

28. Zekzer D, Wong FS, Wen L, Altieri M, Gurlo T, von Grafenstein H, Sherwin RS: Inhibition of diabetes by an insulin-reactive CD4 T-cell clone in the nonobese diabetic mouse. Diabetes 1997;46:1124-1132
29. Wong FS, Karttunen J, Dumont C, Wen L, Visintin I, Pilip IM, Shastri N, Pamer EG, Janeway CA: Identification of an MHC class I-restricted autoantigen in type 1 diabetes by screening an organ-specific cDNA library. Nat Med 1999;5:1026-1031
30. Nakayama M, Abiru N, Moriyama H, Babaya N, Liu E, Miao D, Yu L, Wegmann DR, Hutton JC, Elliott JF, Eisenbarth GS: Prime role for an insulin epitope in the development of type 1 diabetes in NOD mice. Nature 2005;435:220-223
31. Thébault-Baumont K, Dubois-Laforgue D, Krief P, Briand JP, Halbout P, Vallon-Geoffroy K, Morin J, Laloux V, Lehuen A, Carel JC, Jami J, Muller S, Boitard C: Acceleration of type 1 diabetes mellitus in proinsulin 2-deficient NOD mice. J Clin Invest 2003;111:851-857
32. Wong FS, Visintin I, Wen L, Flavell RA, Janeway CA: CD8 T cell clones from young nonobese diabetic (NOD) islets can transfer rapid onset of diabetes in NOD mice in the absence of CD4 cells. J Exp Med 1996;183:67-76
33. Lieberman SM, Takaki T, Han B, Santamaria P, Serreze DV, DiLorenzo TP: Individual nonobese diabetic mice exhibit unique patterns of CD8+ T cell reactivity to three islet antigens, including the newly identified widely expressed dystrophia myotonica kinase. J Immunol 2004;173:6727-6734
34. Pearson JA, Thayer TC, McLaren JE, Ladell K, De Leenheer E, Phillips A, Davies J, Kakabadse D, Miners K, Morgan P, Wen L, Price DA, Wong FS: Proinsulin Expression Shapes the TCR Repertoire but Fails to Control the Development of Low-Avidity Insulin-Reactive CD8+ T Cells. Diabetes 2016;65:1679-1689
35. Wong FS, Siew LK, Scott G, Thomas IJ, Chapman S, Viret C, Wen L: Activation of insulin-reactive CD8 T-cells for development of autoimmune diabetes. Diabetes 2009;58:1156-1164
36. Thayer TC, Pearson JA, De Leenheer E, Hanna SJ, Boldison J, Davies J, Tsui A, Ahmed S, Easton P, Siew LK, Wen L, Wong FS: Peripheral Proinsulin Expression Controls Low-Avidity Proinsulin-Reactive CD8 T Cells in Type 1 Diabetes. Diabetes 2016;65:3429-3439
37. Pearson JA, Wong FS: Identification of Islet Antigen-Specific CD8 T Cells Using MHCI-Peptide Tetramer Reagents in the Non Obese Diabetic (NOD) Mouse Model of Type 1 Diabetes. Methods Mol Biol 2016;1433:119-125
38. Verdaguer J, Schmidt D, Amrani A, Anderson B, Averill N, Santamaria P: Spontaneous autoimmune diabetes in monoclonal T cell nonobese diabetic mice. J Exp Med 1997;186:1663-1676
39. Horai R, Zárate-Bladés CR, Dillenburg-Pilla P, Chen J, Kielczewski JL, Silver PB, Jittayasothorn Y, Chan CC, Yamane H, Honda K, Caspi RR: Microbiota-Dependent Activation of an Autoreactive T Cell Receptor Provokes Autoimmunity in an Immunologically Privileged Site. Immunity 2015;43:343-353
40. Hebbandi Nanjundappa R, Ronchi F, Wang J, Clemente-Casares X, Yamanouchi J, Sokke Umeshappa C, Yang Y, Blanco J, Bassolas-Molina H, Salas A, Khan H, Slattery RM, Wyss M, Mooser C, Macpherson AJ, Sycuro LK, Serra P, McKay DM, McCoy KD,

Santamaria P: A Gut Microbial Mimic that Hijacks Diabetogenic Autoreactivity to Suppress Colitis. Cell 2017;171:655-667.e617
41. Sung SS, Fu SM, Rose CE, Gaskin F, Ju ST, Beaty SR: A major lung CD103 (alphaE)-beta7 integrin-positive epithelial dendritic cell population expressing Langerin and tight junction proteins. J Immunol 2006;176:2161-2172
42. Fonseca DM, Hand TW, Han SJ, Gerner MY, Glatman Zaretsky A, Byrd AL, Harrison OJ, Ortiz AM, Quinones M, Trinchieri G, Brenchley JM, Brodsky IE, Germain RN, Randolph GJ, Belkaid Y: Microbiota-Dependent Sequelae of Acute Infection Compromise Tissue-Specific Immunity. Cell 2015;163:354-366
43. Saxena V, Ondr JK, Magnusen AF, Munn DH, Katz JD: The countervailing actions of myeloid and plasmacytoid dendritic cells control autoimmune diabetes in the nonobese diabetic mouse. J Immunol 2007;179:5041-5053
44. Fukuda S, Toh H, Hase K, Oshima K, Nakanishi Y, Yoshimura K, Tobe T, Clarke JM, Topping DL, Suzuki T, Taylor TD, Itoh K, Kikuchi J, Morita H, Hattori M, Ohno H: Bifidobacteria can protect from enteropathogenic infection through production of acetate. Nature 2011;469:543-547
45. Lam YY, Ha CW, Campbell CR, Mitchell AJ, Dinudom A, Oscarsson J, Cook DI, Hunt NH, Caterson ID, Holmes AJ, Storlien LH: Increased gut permeability and microbiota change associate with mesenteric fat inflammation and metabolic dysfunction in diet-induced obese mice. PLoS One 2012;7:e34233
46. Hsieh CS, Zheng Y, Liang Y, Fontenot JD, Rudensky AY: An intersection between the self-reactive regulatory and nonregulatory T cell receptor repertoires. Nat Immunol 2006;7:401-410
47. Lathrop SK, Bloom SM, Rao SM, Nutsch K, Lio CW, Santacruz N, Peterson DA, Stappenbeck TS, Hsieh CS: Peripheral education of the immune system by colonic commensal microbiota. Nature 2011;478:250-254
48. Cebula A, Seweryn M, Rempala GA, Pabla SS, McIndoe RA, Denning TL, Bry L, Kraj P, Kisielow P, Ignatowicz L: Thymus-derived regulatory T cells contribute to tolerance to commensal microbiota. Nature 2013;497:258-262
49. Yurkovetskiy L, Burrows M, Khan AA, Graham L, Volchkov P, Becker L, Antonopoulos D, Umesaki Y, Chervonsky AV: Gender bias in autoimmunity is influenced by microbiota. Immunity 2013;39:400-412
50. Markle JG, Frank DN, Mortin-Toth S, Robertson CE, Feazel LM, Rolle-Kampczyk U, von Bergen M, McCoy KD, Macpherson AJ, Danska JS: Sex differences in the gut microbiome drive hormone-dependent regulation of autoimmunity. Science 2013;339:1084-1088
51. Wooldridge L, Ekeruche-Makinde J, van den Berg HA, Skowera A, Miles JJ, Tan MP, Dolton G, Clement M, Llewellyn-Lacey S, Price DA, Peakman M, Sewell AK: A single autoimmune T cell receptor recognizes more than a million different peptides. J Biol Chem 2012;287:1168-1177

Abbreviations

Dendritic cells – DCs

Interferon - IFN

Non-Obese Diabetic mouse - NOD

Proinsulin2 – PI2

Regulatory T-cells - Treg

T-cell receptor – TCR

Figure Legends

Figure 1

Experimental design and spontaneous diabetes development. A; The experimental schema of enrofloxacin treatment, whereby *A22Cα*$^{-/-}$*PI2*$^{-/-}$NOD breeder mice (10 different breeder pairs were used) were either enrofloxacin-treated (top) or untreated (bottom). *A22Cα*$^{-/-}$*PI2*$^{-/-}$NOD litters from these breeders were then randomly chosen and equally divided into enrofloxacin-treated or untreated groups to minimize any breeder effects. B; Diabetes incidence between different enrofloxacin treatment regimens of *A22Cα*$^{-/-}$*PI2*$^{-/-}$NOD mice outlined in A. C; Diabetes incidence of enrofloxacin-treated (from weaning) or untreated mice *A22Cα*$^{-/-}$*PI2*$^{-/-}$ NOD mice. D; Diabetes incidence of enrofloxacin-treated (from weaning) or untreated *G9Cα*$^{-/-}$*PI2*$^{-/-}$NOD mice. Black arrows indicate the time of weaning. Statistical analysis was performed using log-rank test.

Figure 2

Insulin B15-23 T cells are increased in number and activation with Enrofloxacin treatment. A-B; Frequency and absolute number of Insulin B-15-23-reactive CD8+T-cells gated from

live single TCRβ+CD4-CD19-CD11b-CD11c- cells. C & D; Frequency of CD69+ Insulin B-15-23-reactive CD8+T-cell population from the PLN (C) and PP (D). Cells were gated as in (A-B) prior to subsequently gating on CD69. E & F; Frequency of CD44+CD62L-expressing Insulin B-15-23-reactive CD8+T-cells in the PLN (E) and PP (F). Cells were gated as in (A-B), prior to subsequently gating by CD44 and CD62L expression. G-H; Frequency of TCRβ chains expressed by Insulin B-15-23-reactive CD8+T-cells in 6-week old *A22Cα*$^{-/-}$*PI2*$^{-/-}$NOD mice by enrofloxacin treatment (n=7-10) in the PLN (G) and PP (H). All statistical analyses were conducted using a Student's t test. Data are presented as mean ± SEM.

Figure 3

Direct *ex vivo* assessment of antigen presenting cell phenotype in untreated and enrofloxacin-treated *A22Cα*$^{-/-}$*PI2*$^{-/-}$NOD mice. CD11c+cells or CD11b+cells were isolated from the spleen of enrofloxacin-treated or untreated *A22Cα*$^{-/-}$*PI2*$^{-/-}$NOD mice and co-cultured *in vitro* with CFSE-labeled G9CD8+T-cells for 72 hours in the presence of insulin B15-23 peptide. A; Frequency of CD11c+CD103+cells gated from live single CD19-TRBV-MHCII+CD11b-F480-cells. B; Frequency of CD11b+CD103+cells gated from live single CD19-TCRβ-MHCII+CD11c-F480+cells. IFN-gamma (C) and IL10 (E) were assessed in CD11c+ cells gated from live single CD19-TCRβ-MHCII+CD11b-F480-cells. IFN-gamma (D) and IL10 (F) were assessed in CD11b+ cells gated from live single CD19-TCRβ-MHCII+CD11c-F480+cells. All cells shown in A-F were from Peyer's patches. G-H; CFSE-labeled G9 CD8+T-cells were co-cultured with CD11c+ cells (G) or CD11b+ cells (H) (from

enrofloxacin-treated or untreated *A22Cα$^{-/-}$PI2$^{-/-}$*NOD mice) in a 1:1 ratio in the presence or absence of Insulin B15-23 peptide for 48 hours. Data shown were corrected for background (cells co-cultured without peptide). All statistical analyses were conducted using a Student's t test. All data were pooled from 2 independent experiments; n=10. Data are presented as mean with SEM. ND (not detected).

Figure 4

Altered microbial composition in *A22Cα$^{-/-}$PI2$^{-/-}$*NOD mice by enrofloxacin treatment and diabetes development. A; Principal Component of Analysis (PCoA) plot of β-diversity from fecal bacteria of 6-week old *A22Cα$^{-/-}$PI2$^{-/-}$*NOD mice that were untreated (n=29) or treated with enrofloxacin (n=35) B; Altered microbiota composition expressed as a percentage of relative abundance of bacterial genus. All bacteria belong to the *Firmicutes* phylum except *Bifidobacterium*, which belongs to the phylum, *Actinobacteria*. C; PCoA plot of β-diversity from fecal bacteria of 6-week old *A22Cα$^{-/-}$PI2$^{-/-}$*NOD mice treated with enrofloxacin that were non-diabetic, (n=25), or diabetic, (n=10) by the end of the observation period (10 weeks of age). D; Altered microbiota composition expressed as a percentage of relative abundance from the genus level except *Bacteroides ovatus* (species level) and *Lachnospiraceae* (family level). *Lachnospiraceae* and *Roseburia* (a member of *Lachnospiraceae*) are both members of the *Firmicutes* phylum; *Bacteroides ovatus* belongs within the *Bacteroidetes* phylum, while *Adlercreutzia* belongs within the *Actinobacteria* phylum. Analysis of similarities (ANOSIM)

was used to analyze β-diversity of taxonomic families of gut microbiota (A & C). B & D were assessed for statistical significance using a Student's t test.

Figure 5

Effect of culture of *A22Cα*$^{-/-}$*PI2*$^{-/-}$NOD mice splenocytes with small intestinal bacteria from untreated or Enrofloxacin-treated mice. Intracellular IFN-gamma was investigated in CD8+T-cells (A-B; gated from TCRβ+CD19-CD4); CD11b+cells (C-D; gated from TCRβ-CD19-IA^{g7}+CD11c-F480+) and CD11c+cells (E-F; gated from TCRβ-CD19-IA^{g7}+CD11b-F480-). Splenocyte donors were studied at both 6- (A, C, E) and 10-weeks of age (B, D, F). Average baseline levels of splenocyte IFN-gamma-producing cells, cultured without bacteria, were similar in all treatment groups are shown by the dotted line. The black bars represent splenocytes from non-Enrofloxacin-treated mice, while the grey bars represent splenocytes from the Enrofloxacin-treated mice. The labeling beneath the graphs represent the origin of the bacteria - Bacteria from Non-Enrofloxacin treated mice labeled as Non-Enrofloxacin-treated bacteria, bacteria from non-diabetic Enrofloxacin-treated mice labeled as Enrofloxacin-treated bacteria (non-diabetic) and bacteria from diabetic Enrofloxacin-treated mice labeled as Enrofloxacin-treated bacteria (diabetic). All splenocyte cultures with bacteria displayed significant differences from those without bacteria. All data was pooled from 3 independent experiments (n=8/group; from 3-4 different breeders). All data were assessed for statistical significance using multiple Student's t tests corrected using FDR. Data are plotted as mean with SEM.

Figure 6

Effect of culture of *G9Cα*$^{-/-}$NOD mice splenocytes with small intestinal bacteria from untreated or enrofloxacin-treated *A22Cα*$^{-/-}$*PI2*$^{-/-}$NOD mice. Intracellular IFN-gamma was measured in CD8+T-cells (A; gated from TCRβ+CD19-CD4-), CD11b+cells (B; gated from TCRβ-CD19-IA^{g7}+CD11c-F480+) and CD11c+cells (C; gated from TCRβ-CD19-IA^{g7}+CD11b-F480-). Average baseline levels of splenocyte IFN-gamma-producing cells, cultured without bacteria, which were similar in all treatment groups are shown by the dotted line. The labeling beneath the graphs represent the origin of the bacteria - Bacteria from Non-Enrofloxacin treated mice labeled as Non-Enrofloxacin-treated bacteria, bacteria from non-diabetic Enrofloxacin-treated mice labeled as Enrofloxacin-treated bacteria (non-diabetic) and bacteria from diabetic Enrofloxacin-treated mice labeled as Enrofloxacin-treated bacteria (diabetic). All splenocyte cultures with bacteria displayed significant differences from those without bacteria. All data was pooled from 2 independent experiments (n=6/group). All data were assessed for statistical significance using multiple Student's t tests corrected using FDR. Data are presented as mean with SEM.

Figure 7

Effect of enrofloxacin treatment on non-TCR restricted polyclonal NOD mice. A; Principal Component of Analysis (PCoA) plot of β-diversity from fecal bacteria of 3- and 6-week old NOD mice that were untreated or treated with enrofloxacin (n=4-7 mice). B; Altered microbiota composition expressed as a percentage of relative abundance of bacterial genus. C; Absolute number of Insulin B-15-23-reactive CD8+T-cells gated from live single

TCRβ+CD4-CD19-CD11b-CD11c- cells. D; Absolute number of CD69+ Insulin B-15-23-reactive CD8+T-cells gated as in (C) prior to subsequently gating on CD69. E-G; Frequency of IFN-gamma producing CD8+T-cells (E; gated from TCRβ+CD19-CD4-)), CD11c+cells (F; gated from TCRβ-CD19-IA^{g7}+CD11b-F480-) and CD11b+cells (G; gated from TCRβ-CD19-IA^{g7}+CD11c-F480+). All data was pooled from 2 independent experiments (n=8/group). All statistical analyses were conducted using a Student's t test. Data are presented as mean ± SEM.

Supplementary Figure Legends

Supplementary Figure 1

Frequencies of CD4+T-cells, CD8+T-cells and Treg cells. A-B; CD4+ and CD8+T-cell frequency in lymphoid tissues (Spleen, Pancreatic draining lymph node (PLN), mesenteric lymph node (MLN) or Peyer's patches (PP) of *A22Cα*$^{-/-}$*PI2*$^{-/-}$NOD mice, gated from total live single cells. C; Frequency of CD4+FoxP3+ Treg cells in the PLN or PP, gated from live single TCRβ+CD19-CD8-cells. Data were pooled from 2 independent experiments (n=10). Statistical analysis was performed using Student's t test. Data shown are plotted as mean with SEM.

Supplementary Figure 2

CD8+T-cell staining with insulin-B15-23 tetramer. A; Representative Insulin B15-23-tetramer (H-$2K^{d}$-LYLVCGERG BV421 tetramer) staining of CD8+T-cells from the PLN,

including a negative control (H-2Kd-AYAAAAAAV-BV421 tetramer) and a positive control (cells from *G9Cα*$^{-/-}$NOD). B; Representative CD69 staining from Insulin-B15-23-reactive CD8+T-cells from PLN and PP gated from live single TCRβ+CD19-CD4-CD8+Tetramer+T-cells. C-D; CD69 expression in Insulin B15-23 Tetramer- CD8+T-cells from PLN (C) and PP (D). E; Representative CD44 and CD62L staining from Insulin-B15-23-reactive CD8+T-cells from PLN and PP gated from live single TCRβ+CD19-CD4-CD8+Tetramer+T-cells. F-G; CD44+CD62L- expression in Insulin B15-23 Tetramer- CD8+T-cells from PLN (F) and PP (G). Data were pooled from 2 independent experiments (n=10). Statistical analysis was performed using Student's t test. Data shown are plotted as mean with SEM.

Supplementary Figure 3

CD8+T-cell staining with anti-TCRVβ antibodies. TCRVβ repertoire differences in total T-cell population in *A22Cα*$^{-/-}$*PI2*$^{-/-}$NOD mice by enrofloxacin treatment in the PLN (A) or PP (B) of age-matched mice (6 to10-week-old). Enrofloxacin-treated mice are shown as those that developed diabetes and those that did not. Statistical analysis was performed using Student's t test. Data shown are plotted as mean with SEM.

Supplementary Figure 4

Representative FACS plots and FMOs for Insulin B15-23-reactive CD8+T-cell staining with anti-TCRVβ antibodies of age-matched *A22Cα*$^{-/-}$*PI2*$^{-/-}$NOD mice (6-week-old) by enrofloxacin treatment. TCRVβ5 (A), TCRVβ6 (B) TCRVβ8 (C), TCRVβ11 (D) and TCRVβ12 (E) cells in the PP are shown. All cells were gated on from live single

TCRβ+CD8+CD4-CD19-InsulinB15-23 tetramer+ cells prior to gating on the cells expressing the particular TCRVβ chain.

Supplementary Figure 5

Direct *ex vivo* assessment of antigen presenting cell phenotype in untreated and enrofloxacin-treated *A22Cα*$^{-/-}$*PI2*$^{-/-}$NOD mice (n=10). A-D; Representative CD103+ staining gated from live single CD19-TCRβ-IA^{g7}+CD11b-F480- cells (A) or CD19-TCRβ-IA^{g7}+CD11c-F480+ cells (B), with cell counts (C-D respectively). E-F; Representative IFN-gamma+ staining gated from live single CD19-TCRβ-IA^{g7}+CD11b-F480-cells (E) or CD19-TCRβ-IA^{g7}+CD11c-F480+ cells (F). G-H; Representative IL10+ staining gated from live single CD19-TCRβ-IA^{g7}+CD11b-F480- cells (G) or CD19-TCRβ-IA^{g7}+CD11c-F480+ cells (H). I-L; Cell counts for IFN-gamma+ CD11c+ cells (I) and CD11b+ cells (J) as well as IL10+ CD11c+ cells (K) and CD11b+ cells (L). All statistical analyses were conducted using a Student's t test. All data were pooled from 2 independent experiments with n=10, Data are presented as mean with SEM. ND (non-detected).

Supplementary Figure 6

Direct *ex vivo* assessment of CD11b+CD11c+ cell phenotype and B-cell IgA frequency in PP of untreated and enrofloxacin-treated *A22Cα*$^{-/-}$*PI2*$^{-/-}$NOD mice. A; Frequency of CD11b+CD11c+CD103+ cells gated from live single CD19-TCRβ-IA^{g7}+CD11b+CD11c+ cells. B-C; Frequency of CD11b+CD11c+IFNgamma+ cells (B) and CD11b+CD11c+IL10+ cells (C) gated as in A. D; Frequency of CD19+IgA+ B-cells gated from live single TCRβ-

IA^{g7}+CD19+ cells. All data were pooled from 2 independent experiments with n=10, Data are presented as mean with SEM.

Supplementary Figure 7

Proliferation of insulin-reactive T cells to peptide presentation by APC from enrofloxacin treated and untreated mice. Representative FACS plots of CFSE-labeled G9 CD8+T-cells showing proliferation in response to Insulin B15-23 peptide presentation by either CD11c+ cells (A) or CD11b+ cells (B) isolated from enrofloxacin treated or untreated *A22Cα*$^{-/-}$*PI2*$^{-/-}$ NOD mice.

Supplementary Figure 8

CD69 and intracellular IFNgamma+ CD8 T cells cultured in the presence of enrofloxacin. G9 CD8+T-cells were co-cultured with irradiated NOD BMDCs for 72 hours in the presence of Insulin B15-23 peptide with or without the addition of different doses of enrofloxacin. Live single cell CD8+T-cells were gated prior to CD69 (A) or IFN-gamma (B) staining. Background values (cells without peptide) were subtracted from all data with peptide. All statistical analyses were conducted using a multiple t test. Data are presented as mean with SEM.

Supplementary Figure 9

Alpha diversity and microbial composition before enrofloxacin treatment at 3 weeks of age, and after treatment at 6 weeks of age in the groups of *A22Cα*$^{-/-}$*PI2*$^{-/-}$NOD mice shown by

enrofloxacin treatment. Fecal bacteria of 3 and 6-week old *A22Cα*$^{-/-}$*PI2*$^{-/-}$NOD mice were sequenced from untreated mice or enrofloxacin-treated (before treatment at 3 weeks of age and after treatment at 6 weeks of age). Samples at 3-weeks of age were collected prior to dividing litters and the start of antibiotic treatment. A; α-diversity as assessed by Chao richness. B; Principal Component of Analysis (PCoA) plot of β-diversity from fecal bacteria of 3 and 6-week old *A22Cα*$^{-/-}$*PI2*$^{-/-}$NOD mice that were untreated or treated from 3 weeks of age. Data shown in A were assessed for statistical significance using a Student's t test. Analysis of similarities (ANOSIM) was used to analyze β-diversity of taxonomic families of gut microbiota (B).

Supplementary Figure 10

Intracellular IFN-gamma+CD8+T-cells in splenocytes from 6 or 10-week-old *A22Cα*$^{-/-}$*PI2*$^{-/-}$ NOD mice cultured with bacteria from untreated and enrofloxacin-treated (both non-diabetic and diabetic) mice. Data show representative staining of IFN-gamma+CD8+T-cells (gated from TCRβ+CD19-CD4-cells) following culture and then stimulation with PMA and ionomycin in the presence of monensin. Each row represents the mouse treatment group at 6 weeks (top 2 rows) and 10 weeks (bottom 2 rows). Each column shows the mouse group from which the bacteria were derived.

Supplementary Figure 11

IFN-gamma+CD11b+cells from splenocytes from 6 or 10-week-old *A22Cα*$^{-/-}$*PI2*$^{-/-}$NOD mice cultured with bacteria from untreated and enrofloxacin-treated (both non-diabetic and

diabetic) mice. Data show representative staining of IFN-gamma+CD11b+cells (gated from TCRβ-CD19-IA^{g7}+CD11c-F480+) following culture and then stimulation with PMA and ionomycin in the presence of monensin. Each row represents the mouse treatment group at 6 weeks (top 2 rows) and 10 weeks (bottom 2 rows). Each column shows the mouse group from which the bacteria were derived..

Supplementary Figure 12

IFN-gamma+CD11c+cells from splenocytes from 6 or 10-week-old *A22Cα*$^{-/-}$*PI2*$^{-/-}$NOD mice cultured with bacteria from untreated and enrofloxacin-treated (both non-diabetic and diabetic) mice. Data show representative staining of IFN-gamma+CD11c+cells (gated from TCRβ-CD19-IA^{g7}+CD11b-F480-) following culture and then stimulation with PMA and ionomycin in the presence of monensin. Each row represents the mouse treatment group at 6 weeks (top 2 rows) and 10 weeks (bottom 2 rows). Each column shows the mouse group from which the bacteria were derived..

Supplementary Figure 13

IFN-gamma secretion from CD8+T-cells, CD11b+cells and CD11c+cells from G9Cα$^{-/-}$NOD splenocytes stimulated with bacteria from untreated and enrofloxacin-treated (both non-diabetic and diabetic) mice. Data show representative staining of IFN-gamma+ CD8+T-cells (A; gated from TCRβ+CD19-CD4-cells), CD11b+cells (B; gated from TCRβ-CD19-IA^{g7}+CD11c-F480+) and CD11c+cells (C; gated from TCRβ-CD19-IA^{g7}+CD11b-F480-) following culture and then stimulation with PMA and ionomycin in the presence of

monensin. Each row represents the mouse treatment group at 6 weeks (top 2 rows) and 10 weeks (bottom 2 rows). Each column shows the mouse group from which the bacteria were derived..

Supplementary Figure 14

Principal Component of Analysis (PCoA) plot of β-diversity from fecal bacteria of 6-week old *A22Cα*$^{-/-}$*PI2*$^{-/-}$NOD mice and NOD mice that were untreated or enrofloxacin-treated from 3 weeks of age. Analysis of similarities (ANOSIM) was used to analyze β-diversity of taxonomic families of gut microbiota. All groups were found to be significantly different to each other (p=0.008).

Supplementary Figure 15

CD8+T-cell staining with insulin-B15-23 tetramer of NOD mice treated or untreated with enrofloxacin. A; Representative Insulin B15-23-tetramer (H-2K^{d}-LYLVCGERG BV421 tetramer) staining of CD8+T-cells, including a negative control (H-2Kd-AYAAAAAAV-BV421 tetramer) and a positive control (*G9Cα*$^{-/-}$NOD cells stained using H-2K^{d}-LYLVCGERG-BV421 tetramer. B; Proportion of insulin-B15-23 tetramer+CD8+T-cells (gated from live single TCRβ+CD19-CD4-CD8+ cells); C; Insulin B15-23-tetramer MFI D; CD69 staining from Insulin-B15-23-reactive CD8+T-cells gated from live single TCRβ+CD19-CD4-CD8+Tetramer+T-cells. E; Representative CD69 staining from insulin-B15-23 tetramer+ CD8+ T-cells. Data were pooled from 2 independent experiments (n=10).

Statistical analysis was performed using Student's t test. Data shown are plotted as mean with SEM.

Supplementary Figure 16

CD8+T-cell staining with IGRP-206-214 tetramer of enrofloxacin-treated and untreated NOD mice. A; Representative IGRP 206-214-tetramer (H-2k^{d}-VYLKTNVFL-APC) staining of CD8+T-cells, including a negative control (H-2Kd-AYAAAAAAV-APC) and a positive control (NY8.3NOD cells stained using H-2k^{d}-VYLKTNVFL-APC tetramer). B-C; Absolute count and frequency of IGRP 206-214-reactive CD8+T-cells gated from live single TCRβ+CD19-CD4-CD8+ cells. D; IGRP 206-214-tetramer MFI. E; CD69 staining from IGRP-206-214-reactive CD8+T-cells gated from live single TCRβ+CD19-CD4-CD8+Tetramer+T-cells. F-G; Frequency and absolute number of CD69+ IGRP 206-214-reactive CD8+T-cells. Data were pooled from 2 independent experiments (n=10). Statistical analysis was performed using Student's t test. Data shown are plotted as mean with SEM.

Supplementary Figure 17

Representative IFN-gamma staining from enrofloxacin-treated and untreated NOD mice (6-weeks of age). A; CD8+T-cells (gated from live single TCRβ+CD19-CD4-cells). B; CD11c+cells (gated from live single TCRβ-CD19-IA^{g7}+CD11b-F480- cells. C; CD11b+cells (gated from live single TCRβ-CD19-IA^{g7}+CD11c-F480+ cells).

A

Enrofloxacin-treated breeders

TRAV8-1/TRAJ9$C\alpha^{-/-}PI2^{-/-}$
(A22$C\alpha^{-/-}PI2^{-/-}$) NOD mice bred

Male mice weaned (3 weeks) and litter divided into two groups

- No further Enrofloxacin treatment (Enrofloxacin-treated until weaning)
- Further Enrofloxacin treatment until termination (Enrofloxacin-treated from birth)

Non-Enrofloxacin-treated breeders

TRAV8-1/TRAJ9$C\alpha^{-/-}PI2^{-/-}$
(A22$C\alpha^{-/-}PI2^{-/-}$) NOD mice bred

Male mice weaned (3 weeks) and litter divided into two groups

- No Enrofloxacin treatment (Non-Enrofloxacin-treated)
- Enrofloxacin treatment until termination (Enrofloxacin-treated from weaning)

B

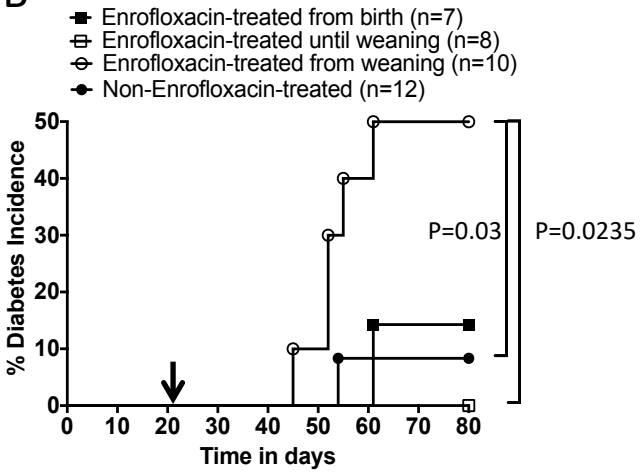

C

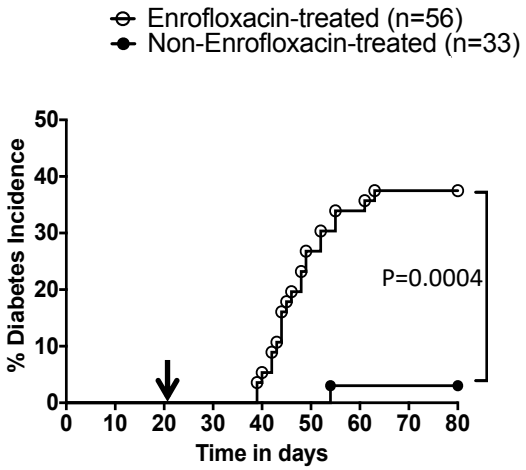

D

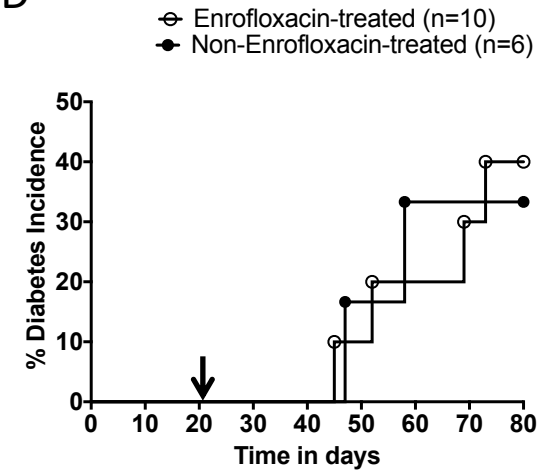

Figure 2

Pearson et al

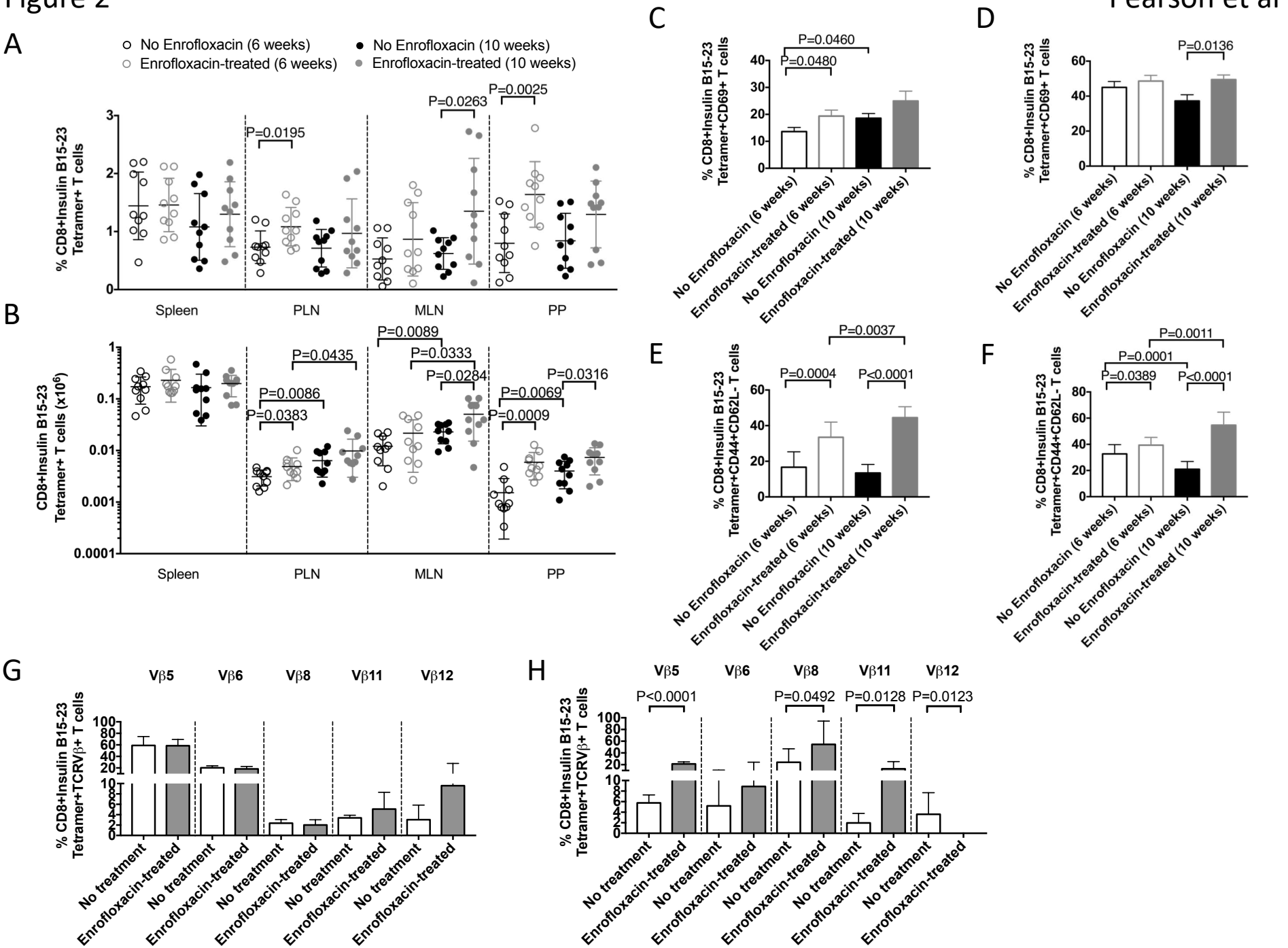

Figure 3

Pearson et al

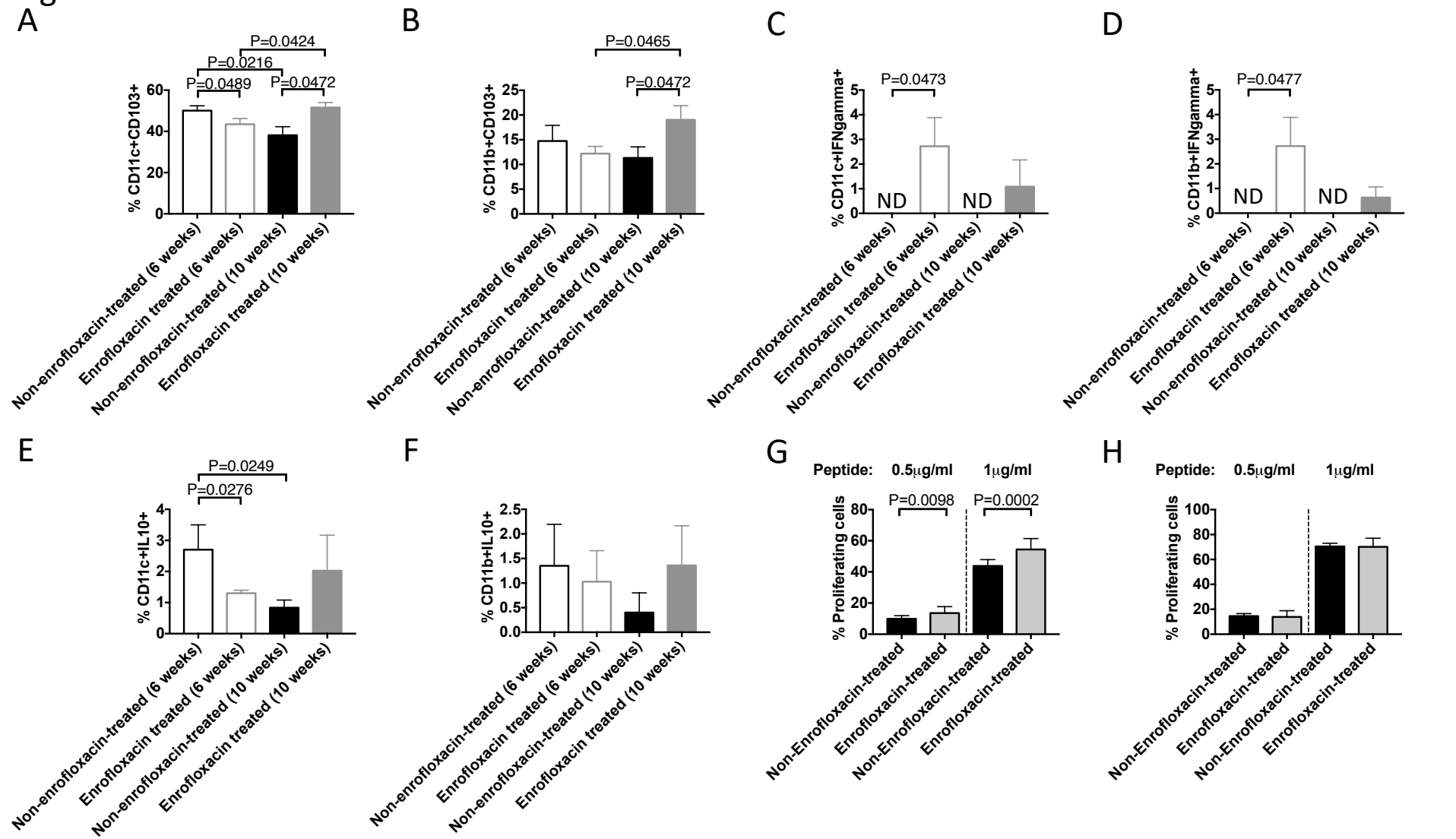

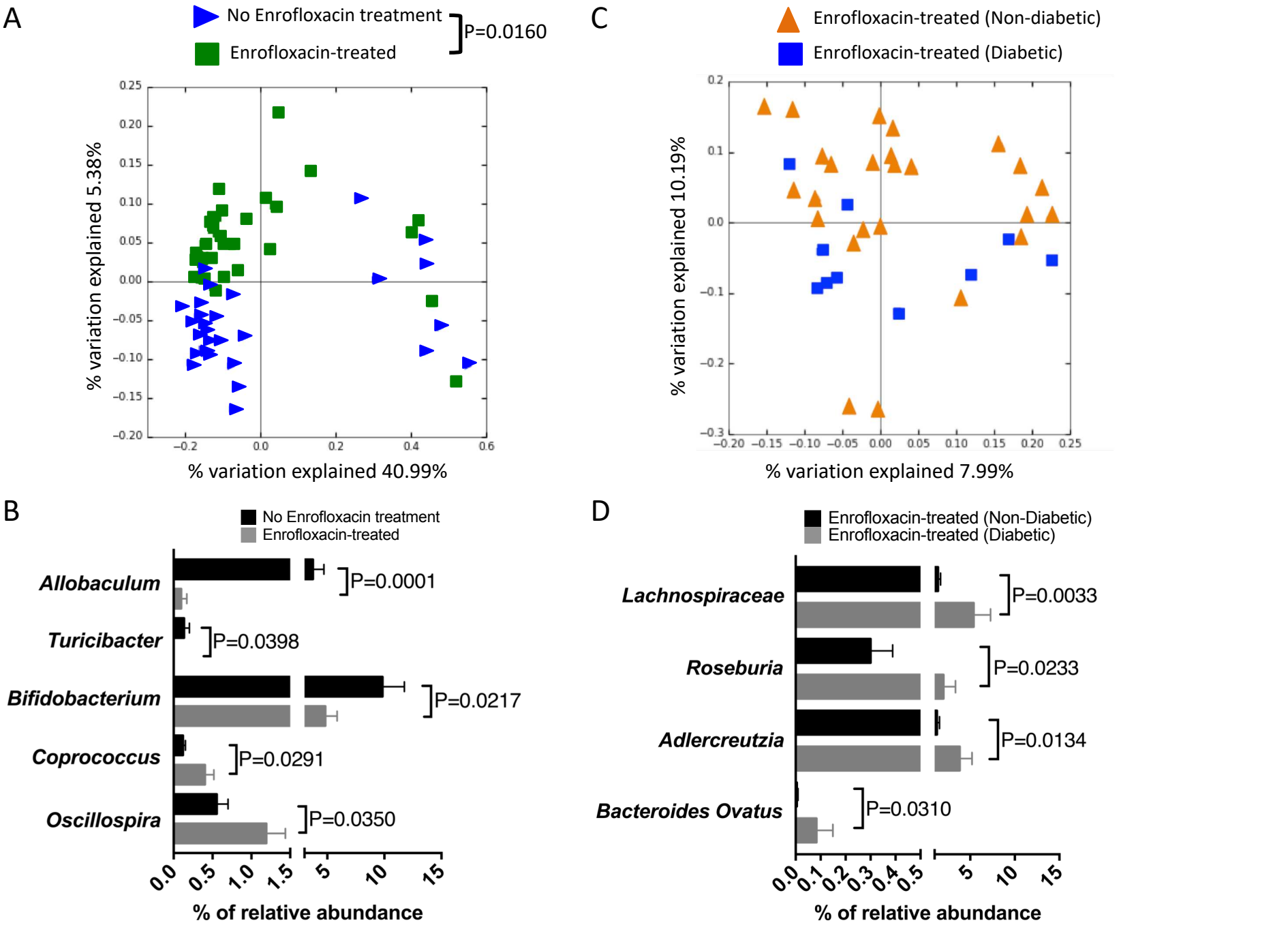
A
No Enrofloxacin treatment
Enrofloxacin-treated
P=0.0160
% variation explained 5.38%
% variation explained 40.99%
C
Enrofloxacin-treated (Non-diabetic)
Enrofloxacin-treated (Diabetic)
% variation explained 10.19%
% variation explained 7.99%
B
No Enrofloxacin treatment
Enrofloxacin-treated
Allobaculum
P=0.0001
Turicibacter
P=0.0398
Bifidobacterium
P=0.0217
Coprococcus
P=0.0291
Oscillospira
P=0.0350
% of relative abundance
D
Enrofloxacin-treated (Non-Diabetic)
Enrofloxacin-treated (Diabetic)
Lachnospiraceae
P=0.0033
Roseburia
P=0.0233
Adlercreutzia
P=0.0134
Bacteroides Ovatus
P=0.0310
% of relative abundance

Figure 5

Pearson et al

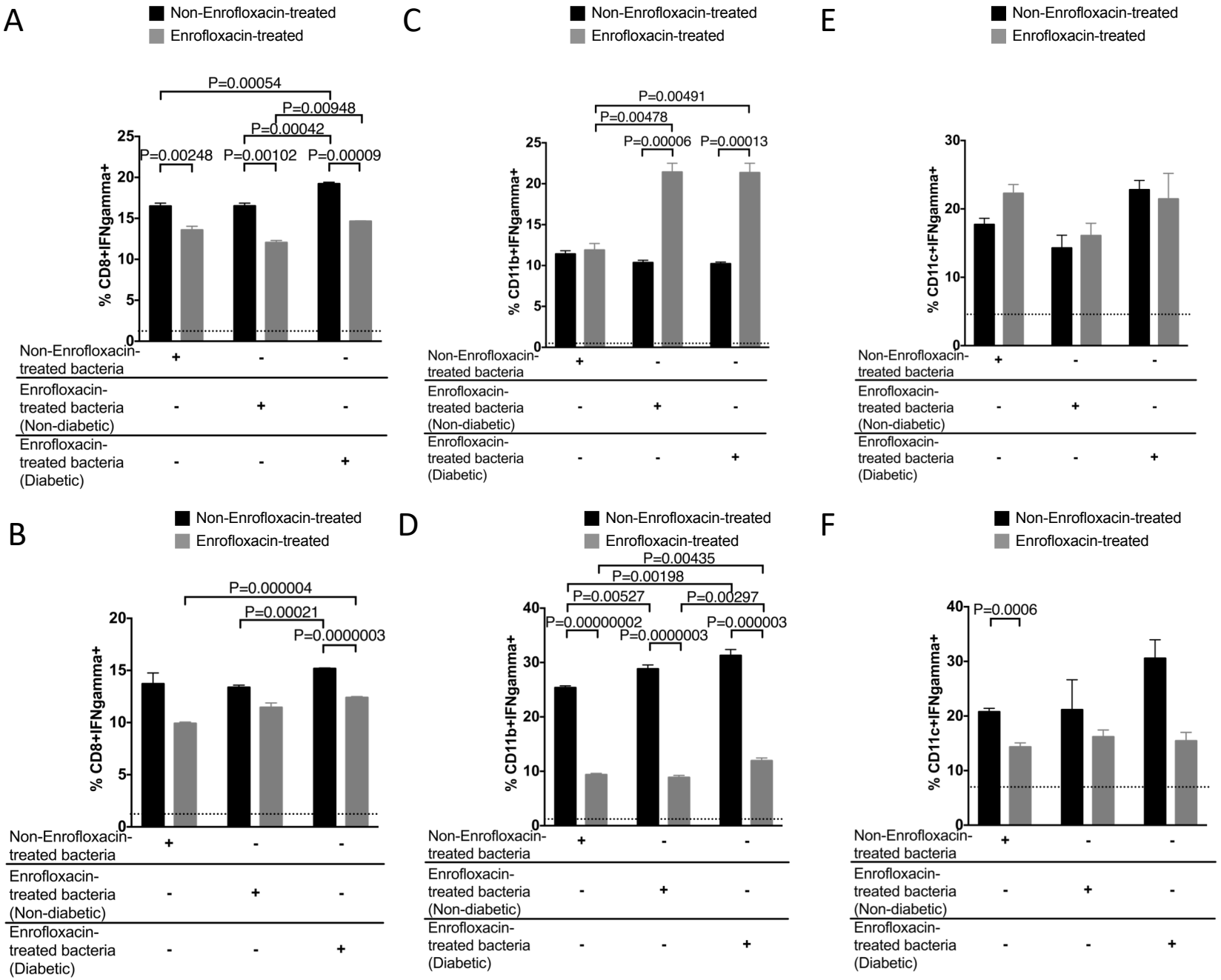

A

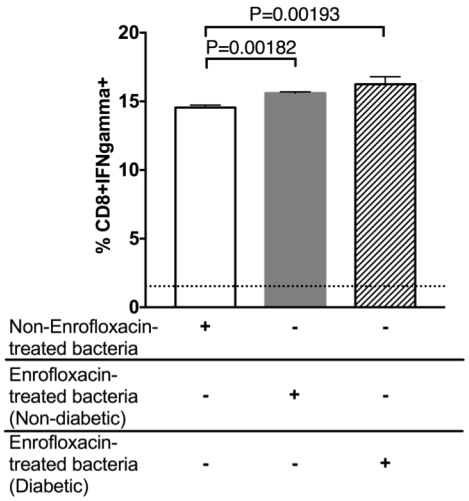
P=0.00193
P=0.00182
% CD8+IFNgamma+
20
15
10
5
0
Non-Enrofloxacin-treated bacteria + - -
Enrofloxacin-treated bacteria (Non-diabetic) - + -
Enrofloxacin-treated bacteria (Diabetic) - - +

B

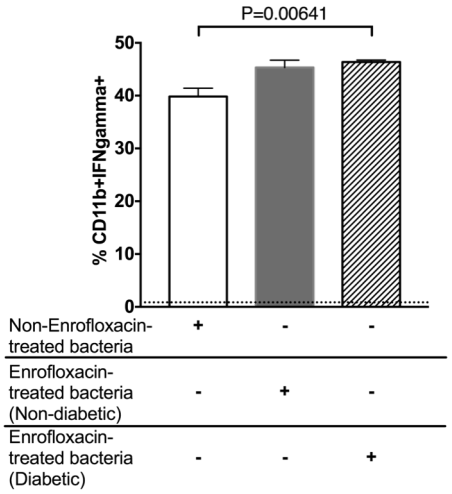
P=0.00641
% CD11b+IFNgamma+
50
40
30
20
10
0
Non-Enrofloxacin-treated bacteria + - -
Enrofloxacin-treated bacteria (Non-diabetic) - + -
Enrofloxacin-treated bacteria (Diabetic) - - +

C

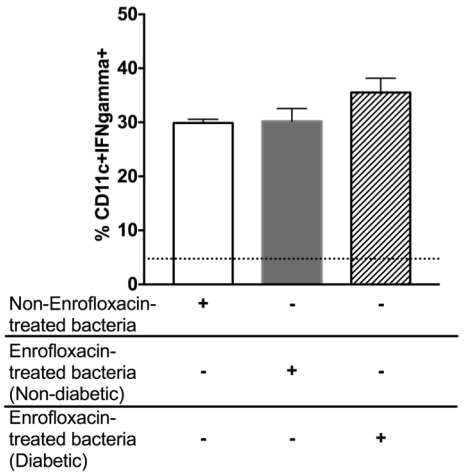
% CD11c+IFNgamma+
50
40
30
20
10
0
Non-Enrofloxacin-treated bacteria + - -
Enrofloxacin-treated bacteria (Non-diabetic) - + -
Enrofloxacin-treated bacteria (Diabetic) - - +

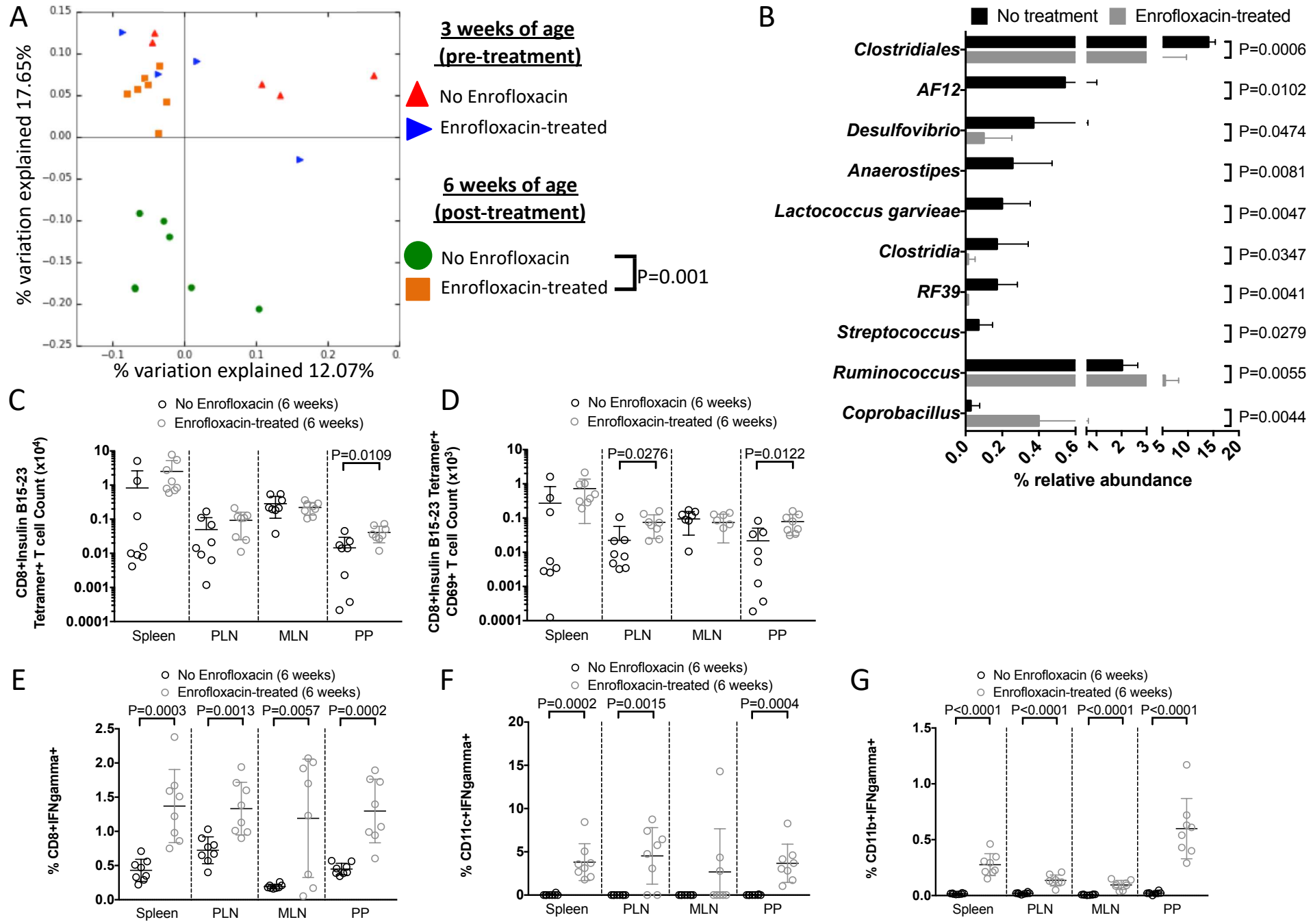
A
% variation explained 17.65%
% variation explained 12.07%
3 weeks of age (pre-treatment)
No Enrofloxacin
Enrofloxacin-treated
6 weeks of age (post-treatment)
No Enrofloxacin
Enrofloxacin-treated
P=0.001
B
No treatment
Enrofloxacin-treated
Clostridiales
AF12
Desulfovibrio
Anaerostipes
Lactococcus garvieae
Clostridia
RF39
Streptococcus
Ruminococcus
Coprobacillus
P=0.0006
P=0.0102
P=0.0474
P=0.0081
P=0.0047
P=0.0347
P=0.0041
P=0.0279
P=0.0055
P=0.0044
% relative abundance
C
No Enrofloxacin (6 weeks)
Enrofloxacin-treated (6 weeks)
CD8+Insulin B15-23 Tetramer+ T cell Count (x10⁴)
P=0.0109
Spleen
PLN
MLN
PP
D
No Enrofloxacin (6 weeks)
Enrofloxacin-treated (6 weeks)
CD8+Insulin B15-23 Tetramer+ CD69+ T cell Count (x10³)
P=0.0276
P=0.0122
Spleen
PLN
MLN
PP
E
No Enrofloxacin (6 weeks)
Enrofloxacin-treated (6 weeks)
% CD8+IFNgamma+
P=0.0003
P=0.0013
P=0.0057
P=0.0002
Spleen
PLN
MLN
PP
F
No Enrofloxacin (6 weeks)
Enrofloxacin-treated (6 weeks)
% CD11c+IFNgamma+
P=0.0002
P=0.0015
P=0.0004
Spleen
PLN
MLN
PP
G
No Enrofloxacin (6 weeks)
Enrofloxacin-treated (6 weeks)
% CD11b+IFNgamma+
P<0.0001
P<0.0001
P<0.0001
P<0.0001
Spleen
PLN
MLN
PP

Supplementary Table 1 – Summary of mouse models used

Strain	TCRα chain	TCRβ chain	Insulin B15-23 reactive CD8+ T-cells	Proinsulin expression	Diabetes incidence	References	Figures
A22Cα$^{-/-}$*PI2*$^{-/-}$NOD	*TRAV8-1 TRAJ9*	Any endogenous TCRβ chain	Up to 3% of the total CD8+ T-cell population	PI2 deficient; PI1 sufficient	25-40% in males	(34)	All (except Fig. 1D, Fig. 6-7, Supp Fig. 8, Supp Fig. 13, Supp Fig. 15-17)
G9Cα$^{-/-}$*PI2*$^{-/-}$NOD	*TRAV8-1 TRAJ9*	*TRBV19 TRBJ2-3*	All T-cells	PI2 deficient; PI1 sufficient	~25-40% in males	(36)	Fig. 1D
G9Cα$^{-/-}$NOD	*TRAV8-1 TRAJ9*	*TRBV19 TRBJ2-3*	All T-cells	PI2 sufficient; PI1 sufficient	None	(35)	Fig. 3G-H, Fig. 6, Supp Fig. 2A, Supp Fig. 8, Supp Fig. 13
NOD	Any endogenous TCRα chain	Any endogenous TCRβ chain	Less than 1% of the total CD8+ T-cell population	PI2 sufficient; PI1 sufficient	20-30% in males	(34)	Fig. 7, Supp Fig. 8, Supp Fig. 14-17

NOD; Non-Obese Diabetic mouse, PI1; Proinsulin 1, PI2; Proinsulin 2, TCR; T-cell Receptor; TRAV; TCRα chain, TRBV; TCRβ chain, TRAJ; TCRα joining chain, TRBJ; TCRβ joining chain.

Supplementary Figure 1

Pearson et al

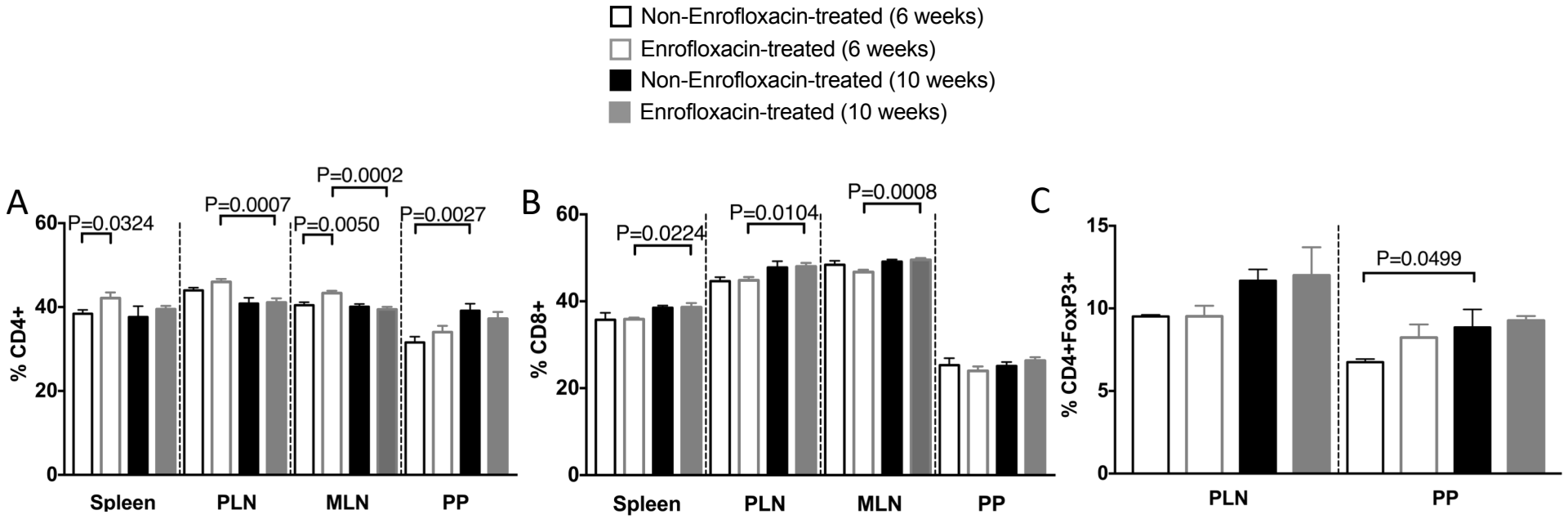

Supplementary Figure 2

Pearson et al

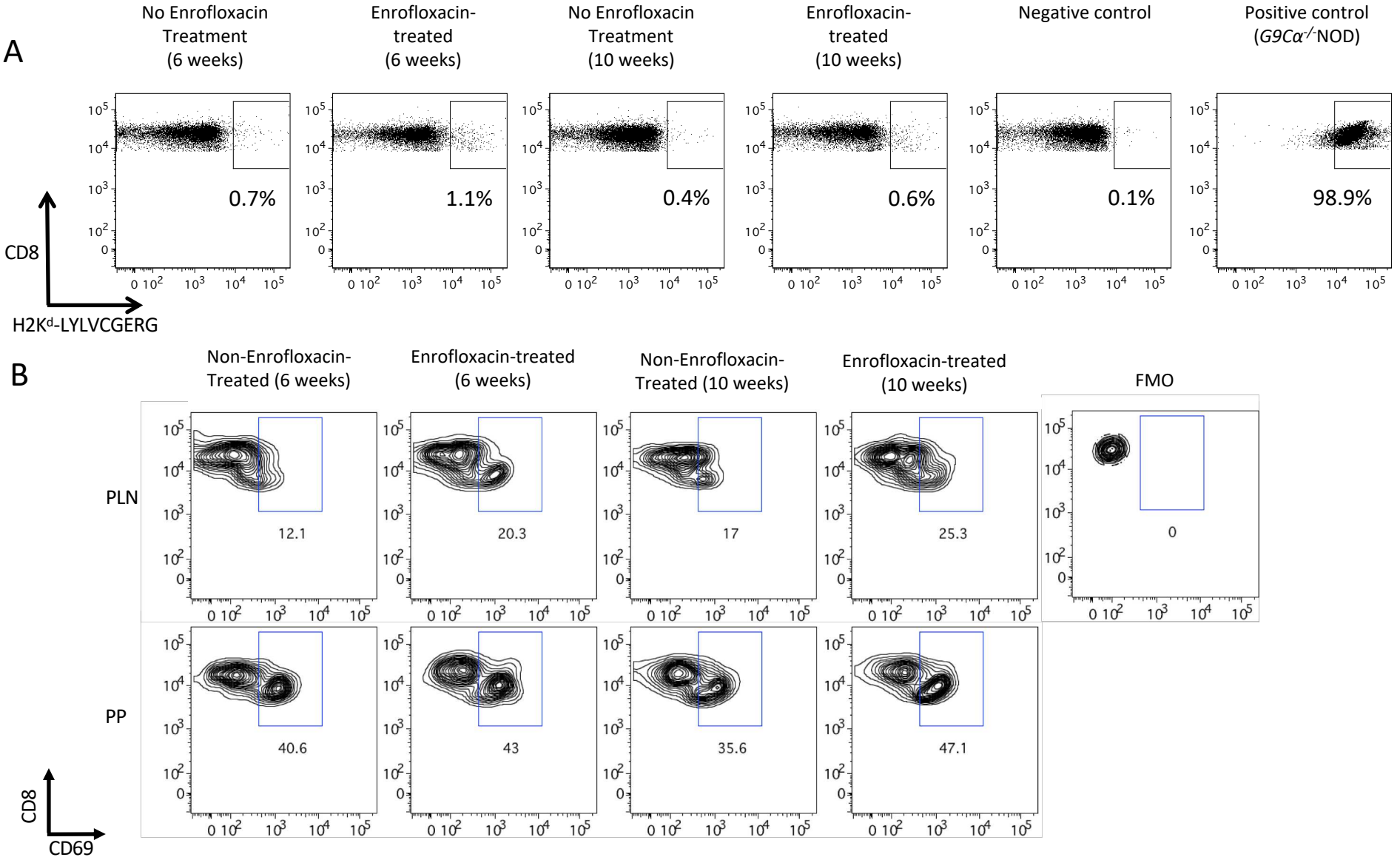

C

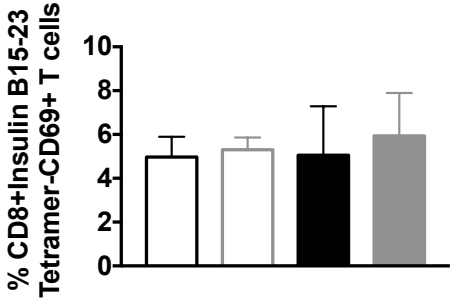
% CD8+Insulin B15-23 Tetramer-CD69+ T cells
10
8
6
4
2
0

D

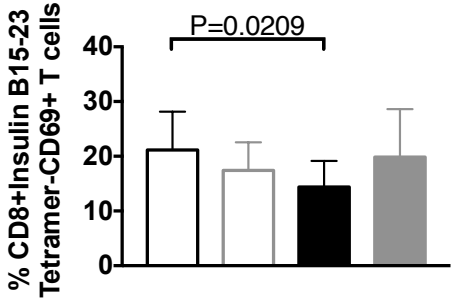
% CD8+Insulin B15-23 Tetramer-CD69+ T cells
P=0.0209
40
30
20
10
0

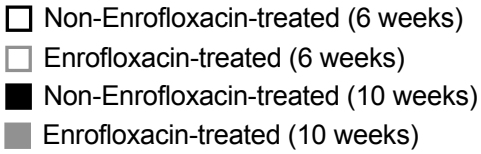
Non-Enrofloxacin-treated (6 weeks)
Enrofloxacin-treated (6 weeks)
Non-Enrofloxacin-treated (10 weeks)
Enrofloxacin-treated (10 weeks)

E

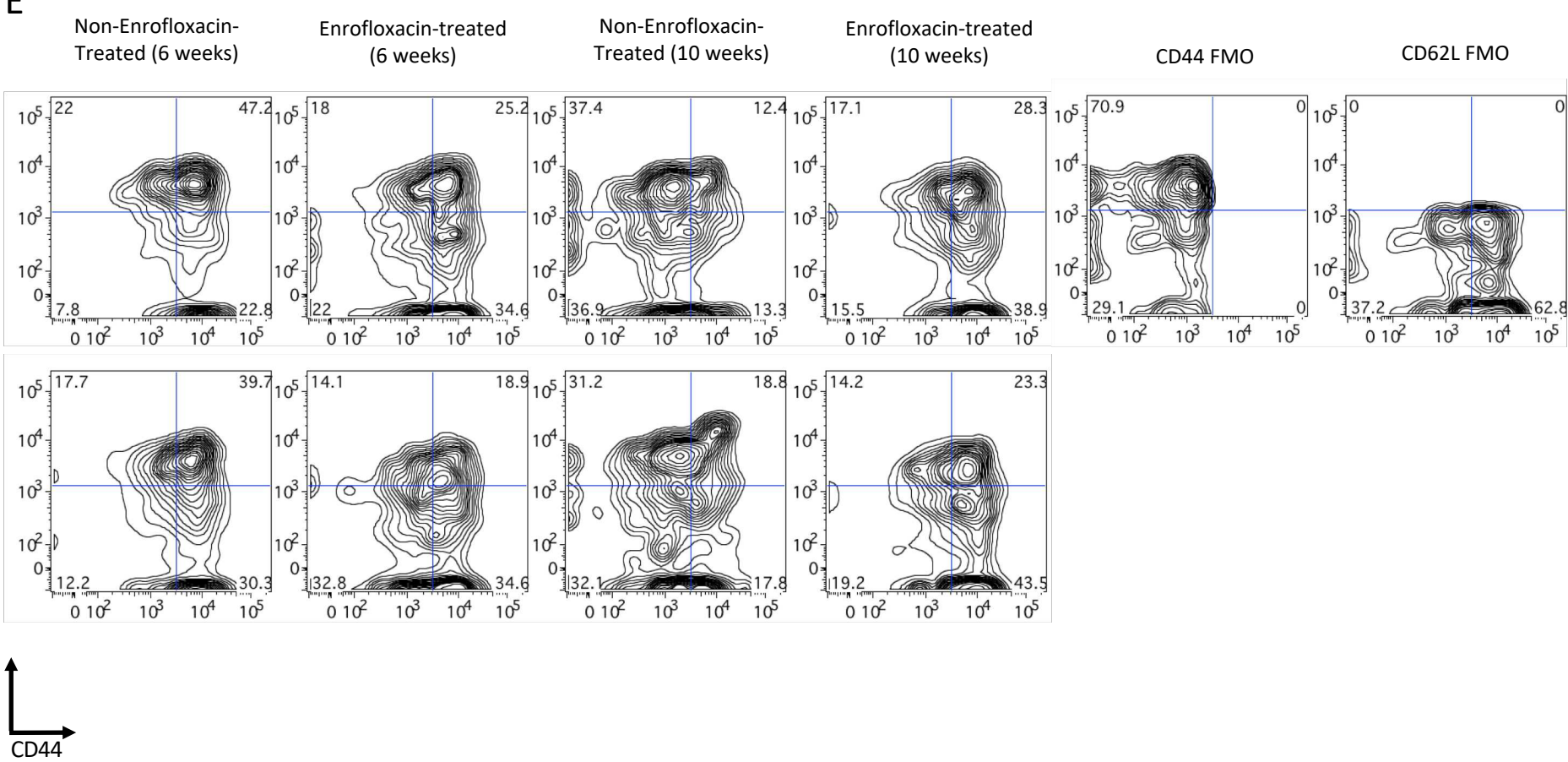
Non-Enrofloxacin-Treated (6 weeks)
Enrofloxacin-treated (6 weeks)
Non-Enrofloxacin-Treated (10 weeks)
Enrofloxacin-treated (10 weeks)
CD44 FMO
CD62L FMO
PLN
PP
22
47.2
7.8
22.8
18
25.2
22
34.6
37.4
12.4
36.9
13.3
17.1
28.3
15.5
38.9
70.9
0
29.1
0
0
0
37.2
62.8
17.7
39.7
12.2
30.3
14.1
18.9
32.8
34.6
31.2
18.8
32.1
17.8
14.2
23.3
19.2
43.5
CD62L
CD44

F

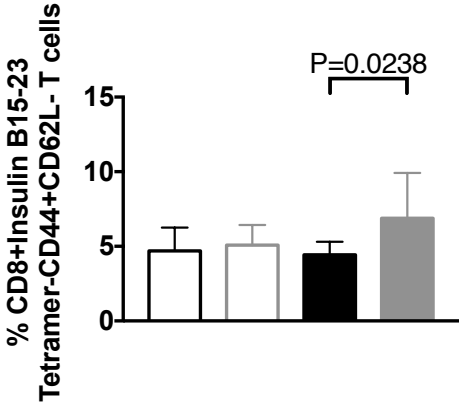
% CD8+Insulin B15-23 Tetramer-CD44+CD62L- T cells
P=0.0238
15
10
5
0

G

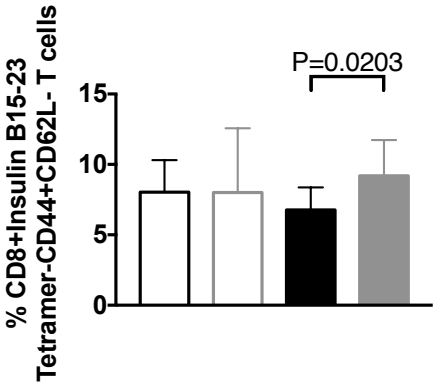
% CD8+Insulin B15-23 Tetramer-CD44+CD62L- T cells
P=0.0203
15
10
5
0

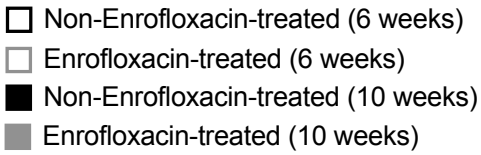
Non-Enrofloxacin-treated (6 weeks)
Enrofloxacin-treated (6 weeks)
Non-Enrofloxacin-treated (10 weeks)
Enrofloxacin-treated (10 weeks)

Supplementary Figure 3

Pearson et al

A

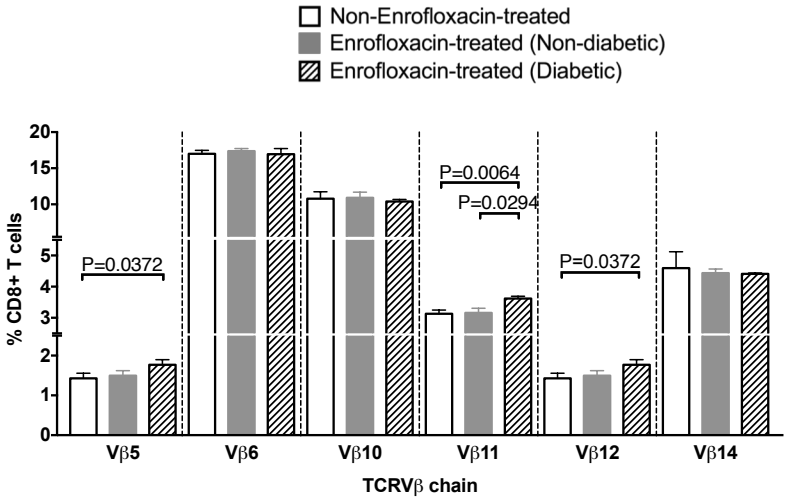

B

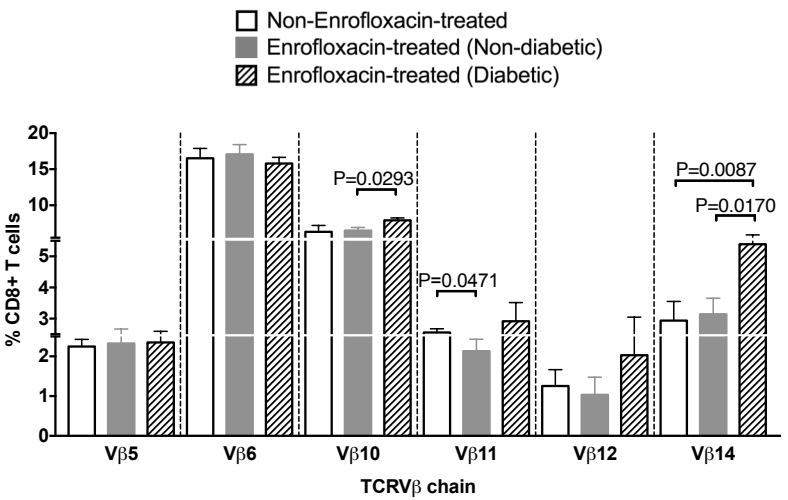

Supplementary Figure 4

Pearson et al

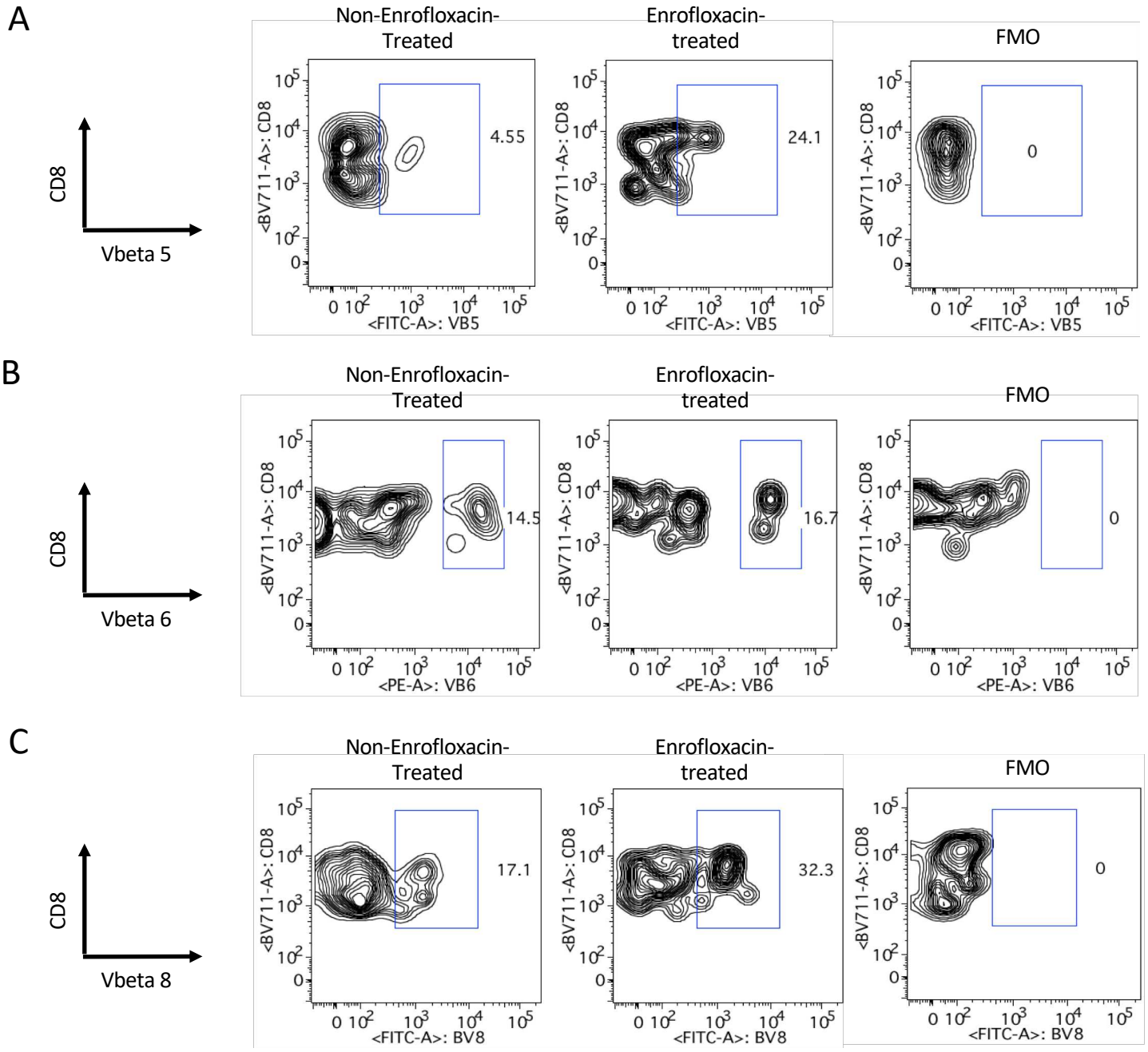

D

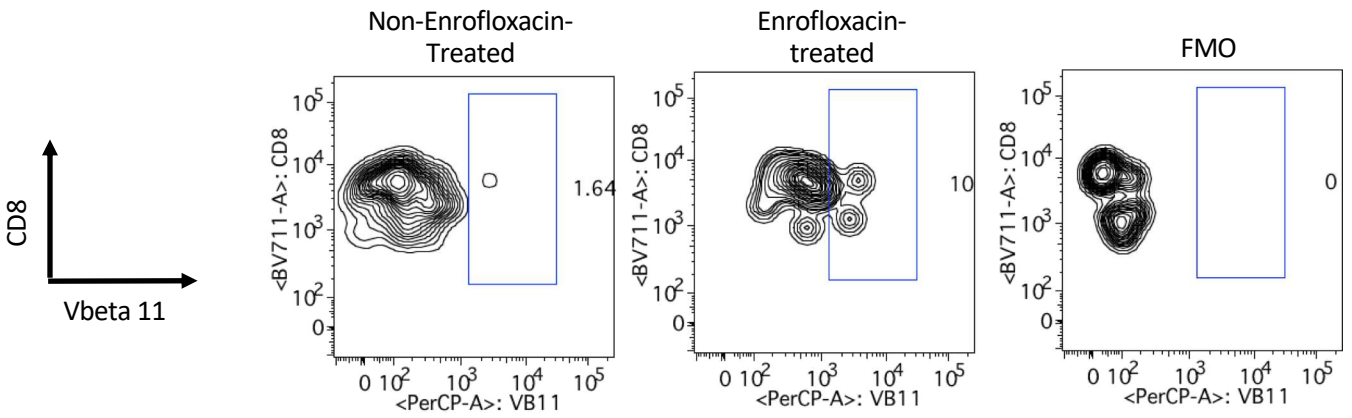
Non-Enrofloxacin-Treated
Enrofloxacin-treated
FMO
CD8
Vbeta 11
<BV711-A>: CD8
<PerCP-A>: VB11
1.64
10
0

E

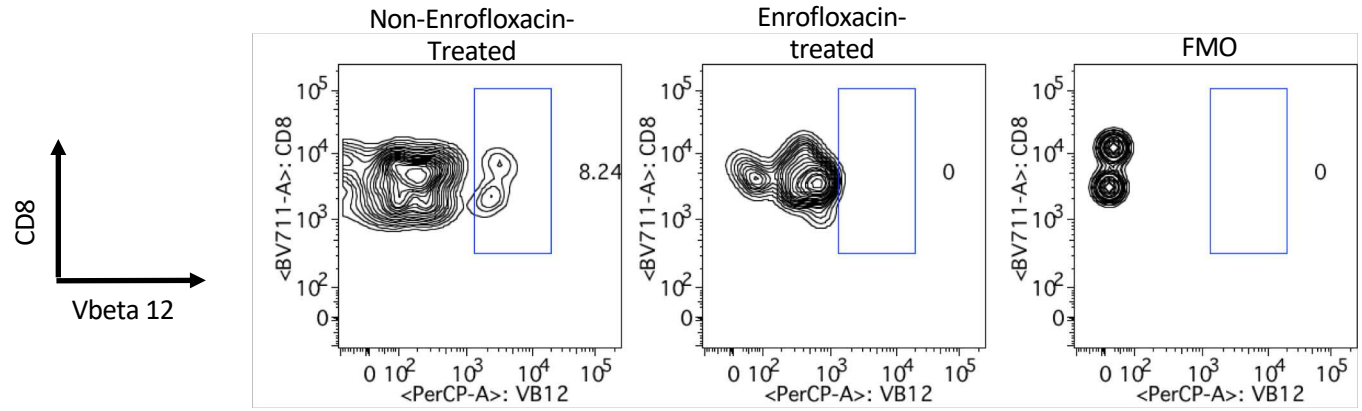
Non-Enrofloxacin-Treated
Enrofloxacin-treated
FMO
CD8
Vbeta 12
<BV711-A>: CD8
<PerCP-A>: VB12
8.24
0
0

Supplementary Figure 5

Pearson et al

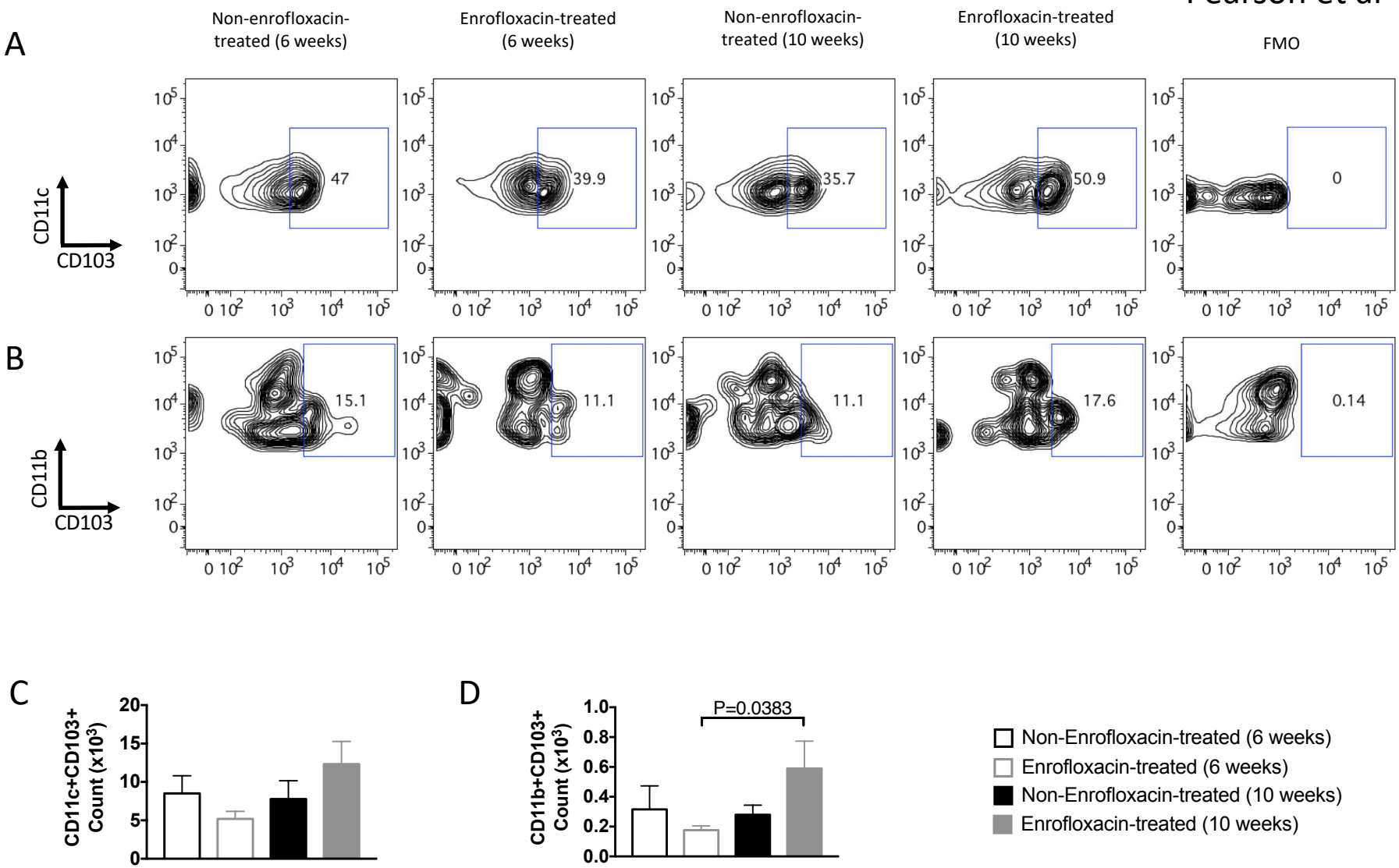

Supplementary Figure 5

Pearson et al

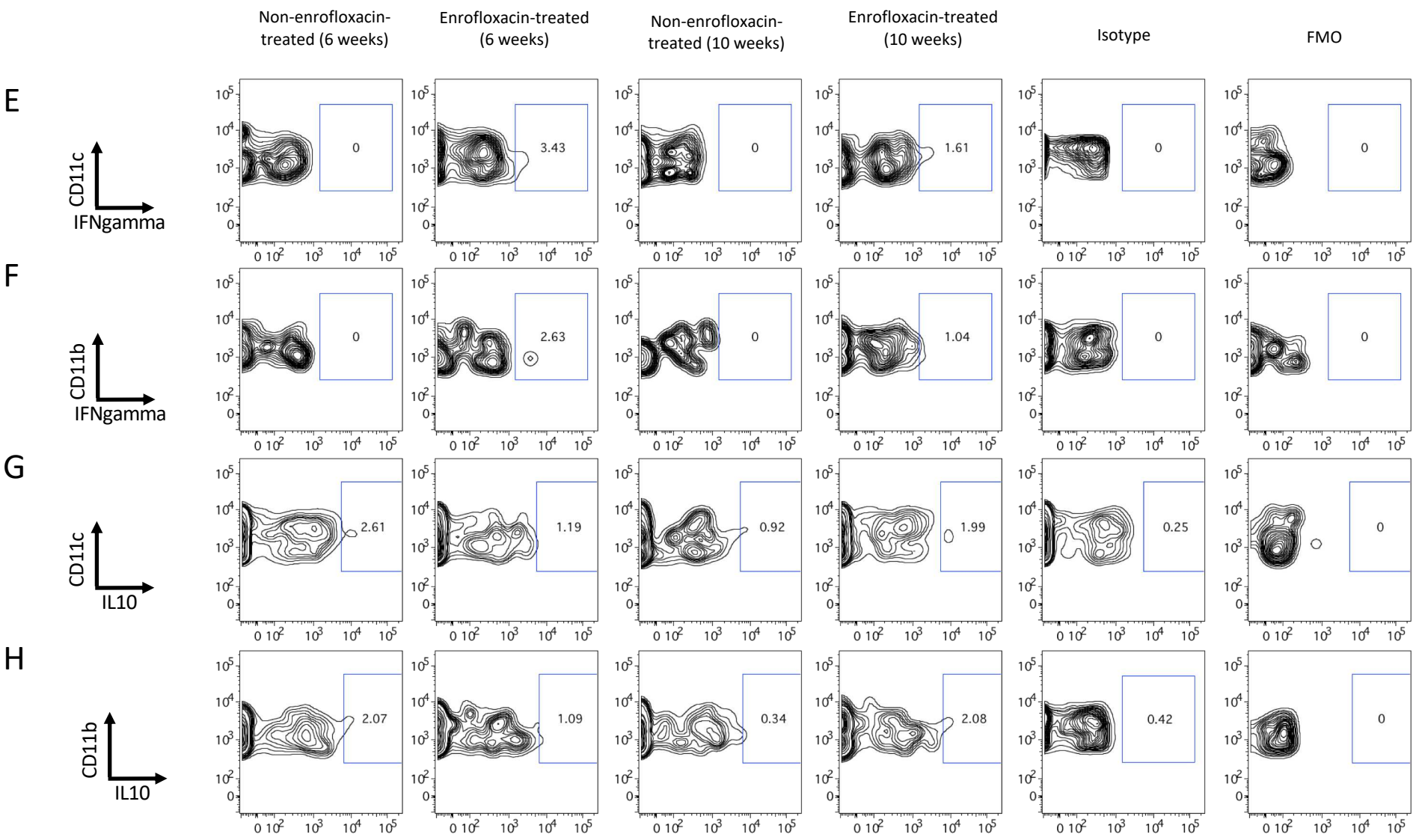

Supplementary Figure 5

Pearson et al

I

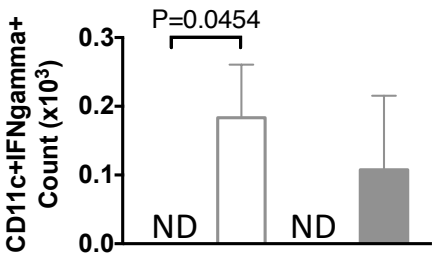

J

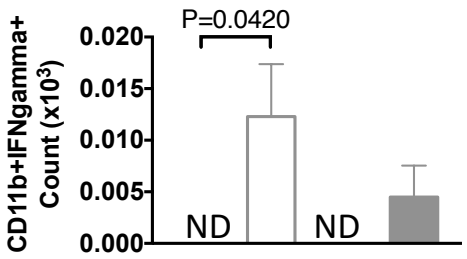

K

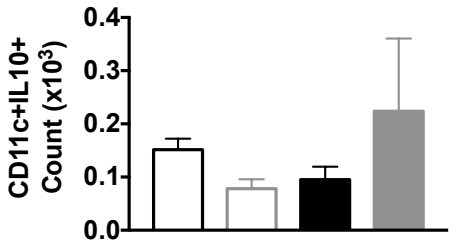

L

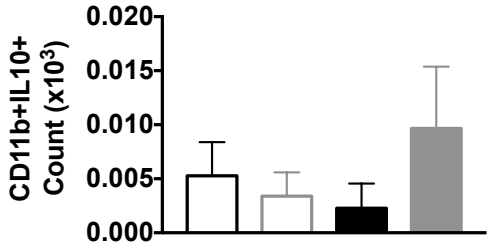

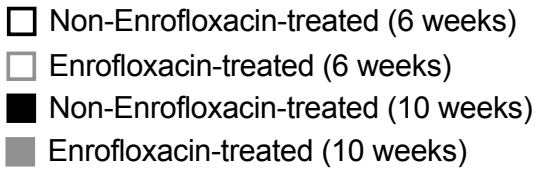

Supplementary Figure 6

Pearson et al

A

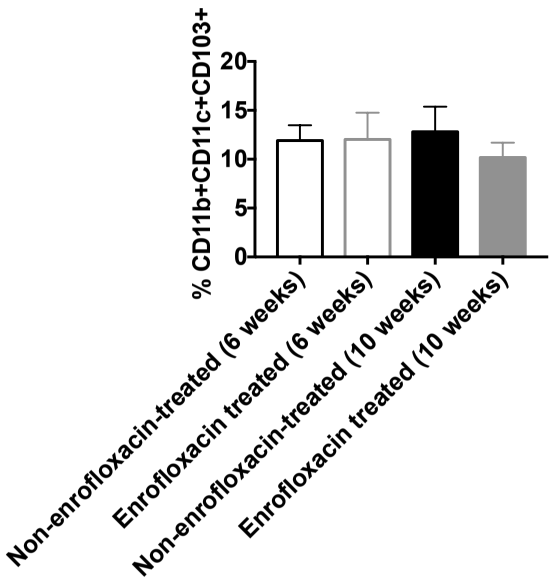

B

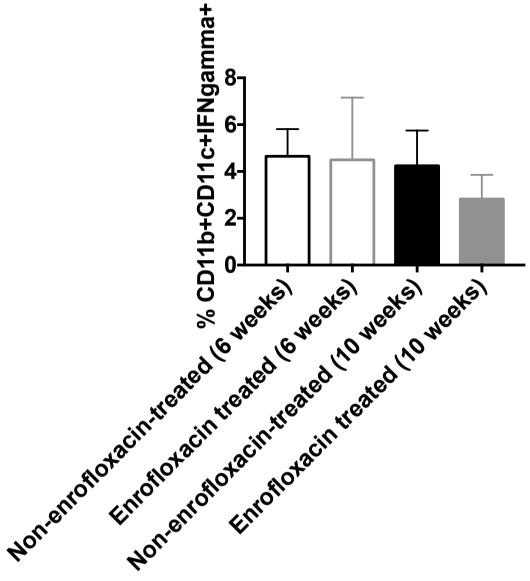

C

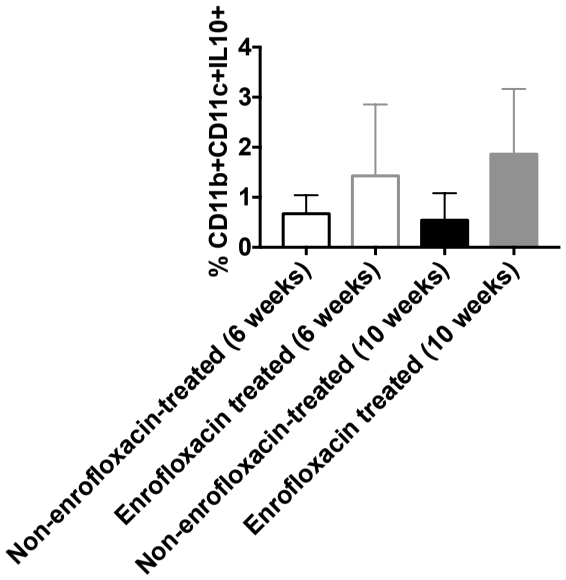

D

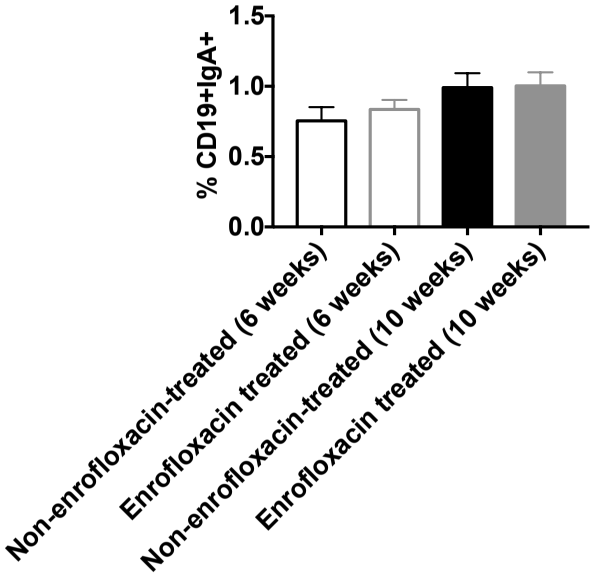

Supplementary Figure 7

Pearson et al

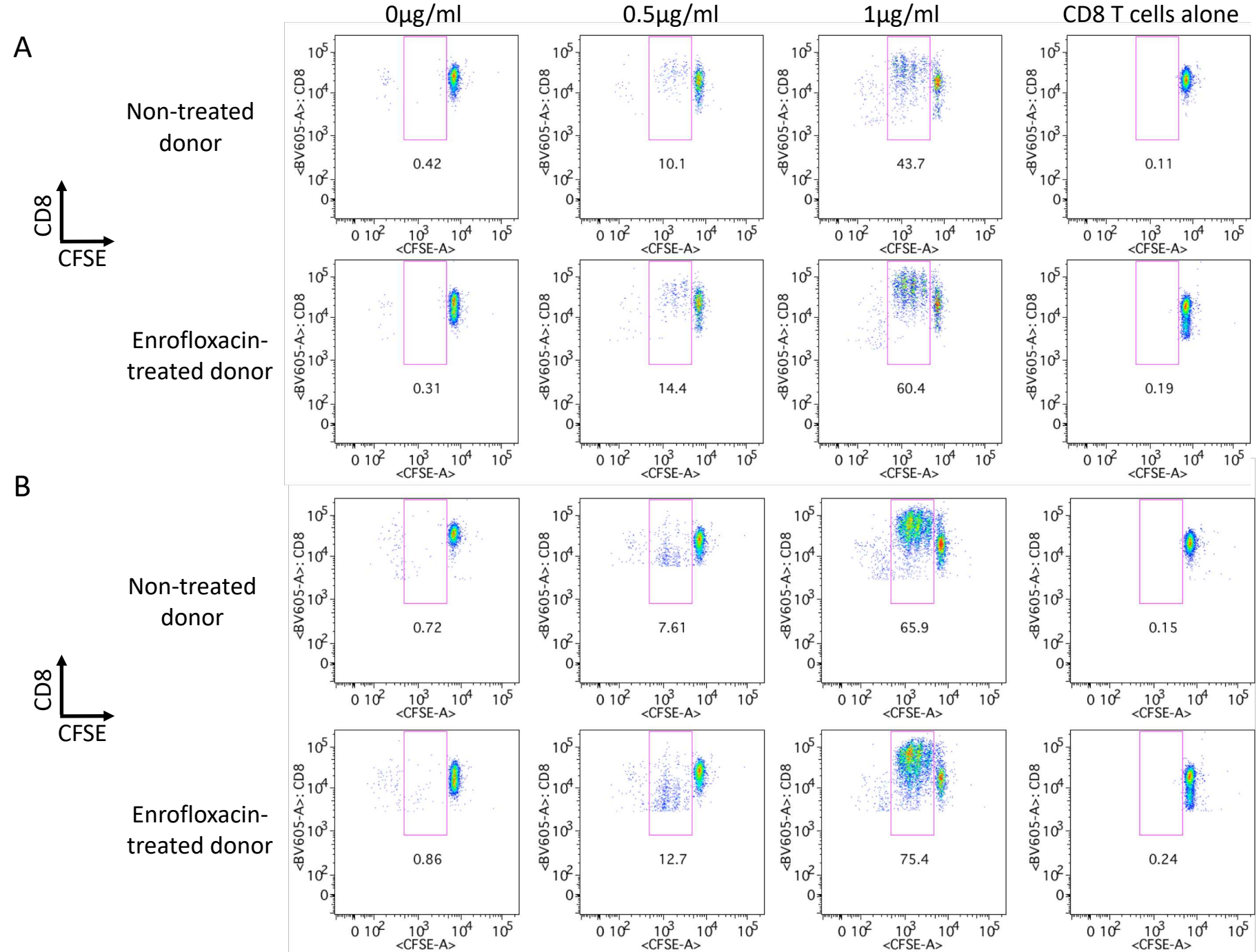

Supplementary Figure 8

Pearson et al

A

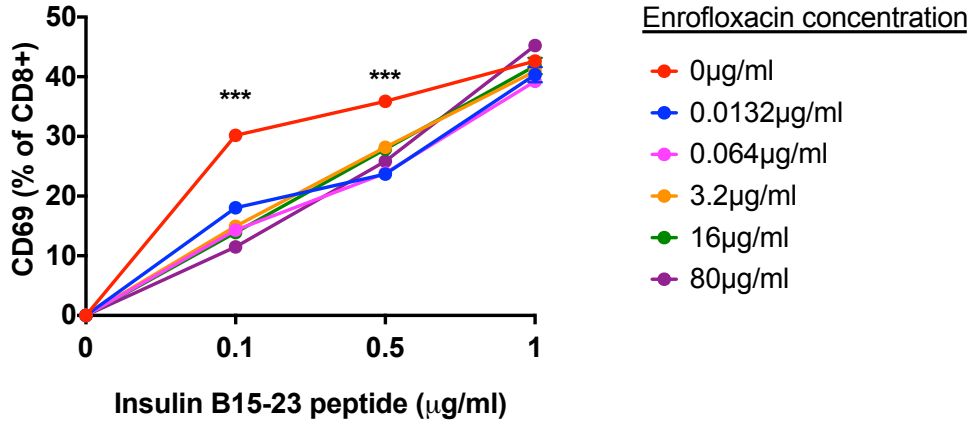

B

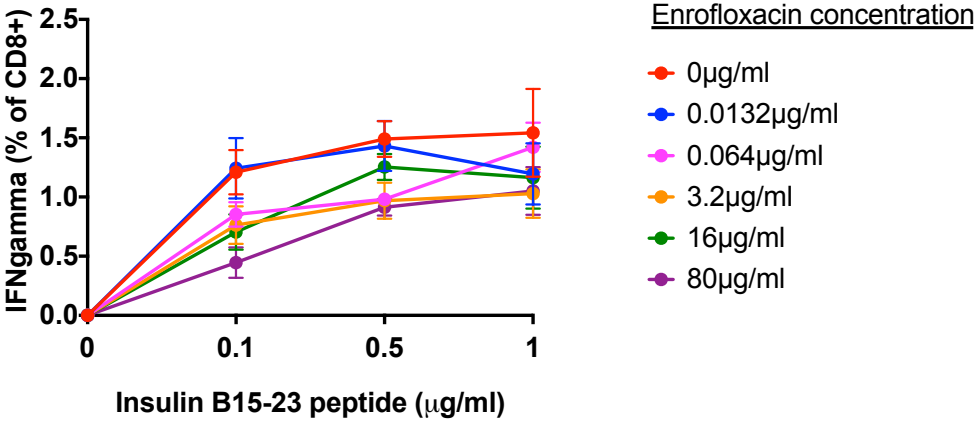

Supplementary Figure 9

Pearson et al

A

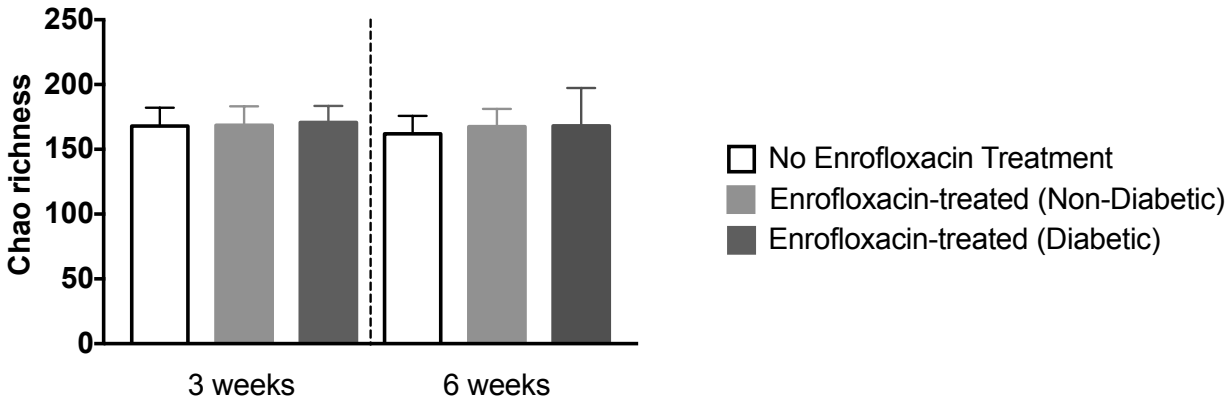

B

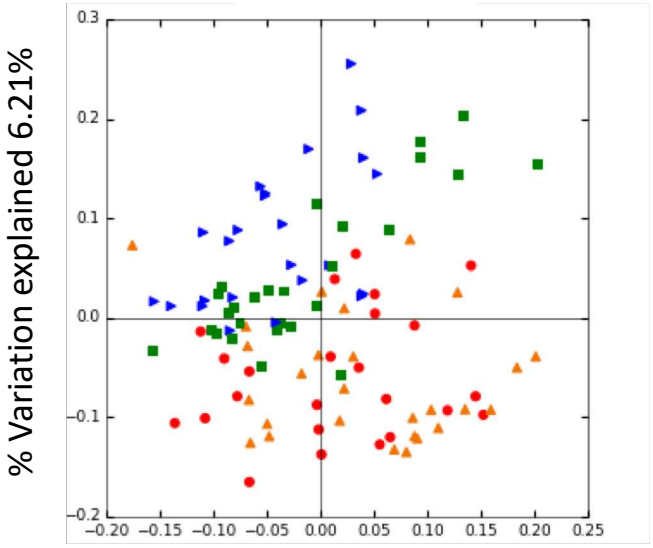

Supplementary Figure 10

Pearson et al

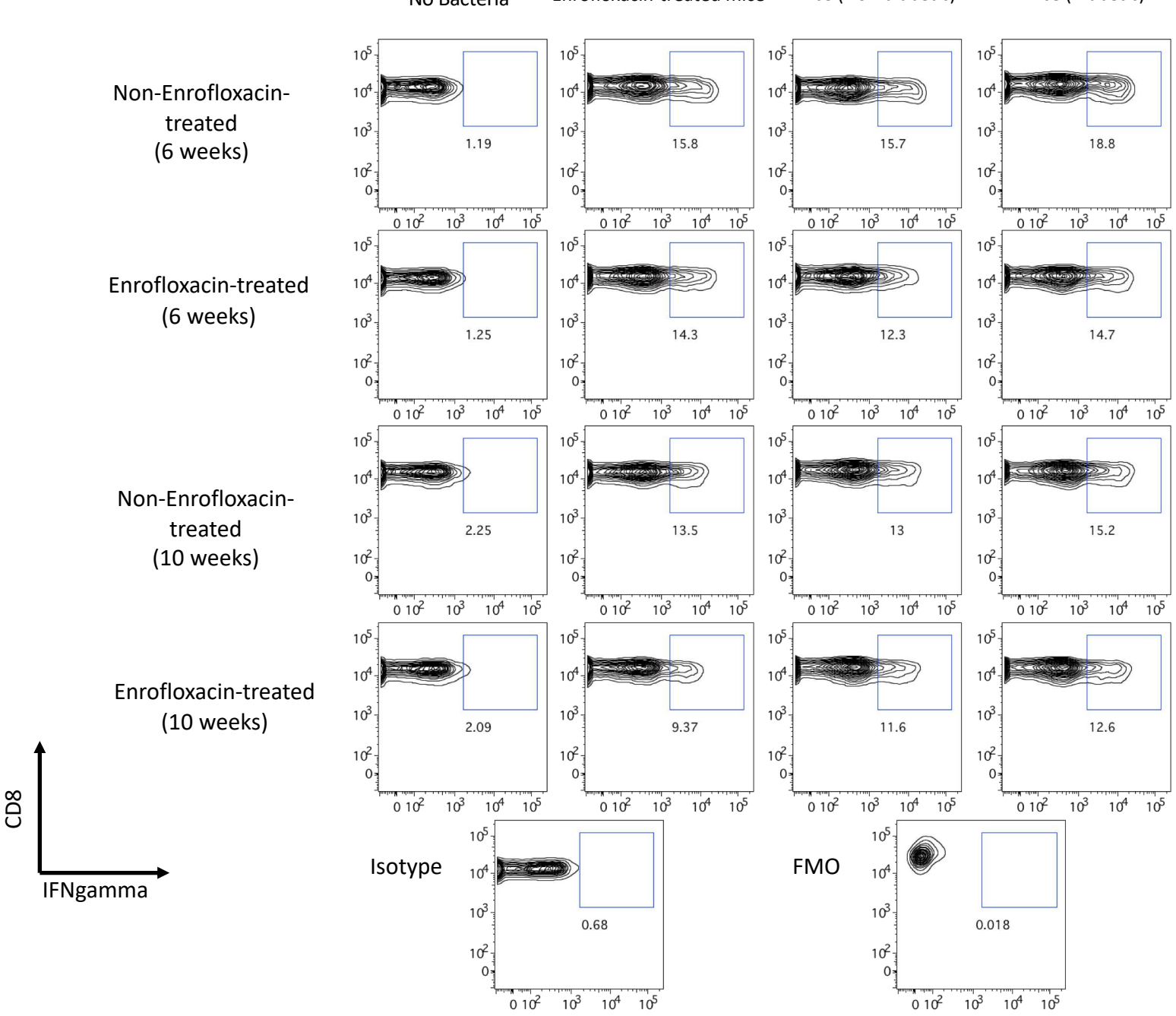

Supplementary Figure 11

Pearson et al

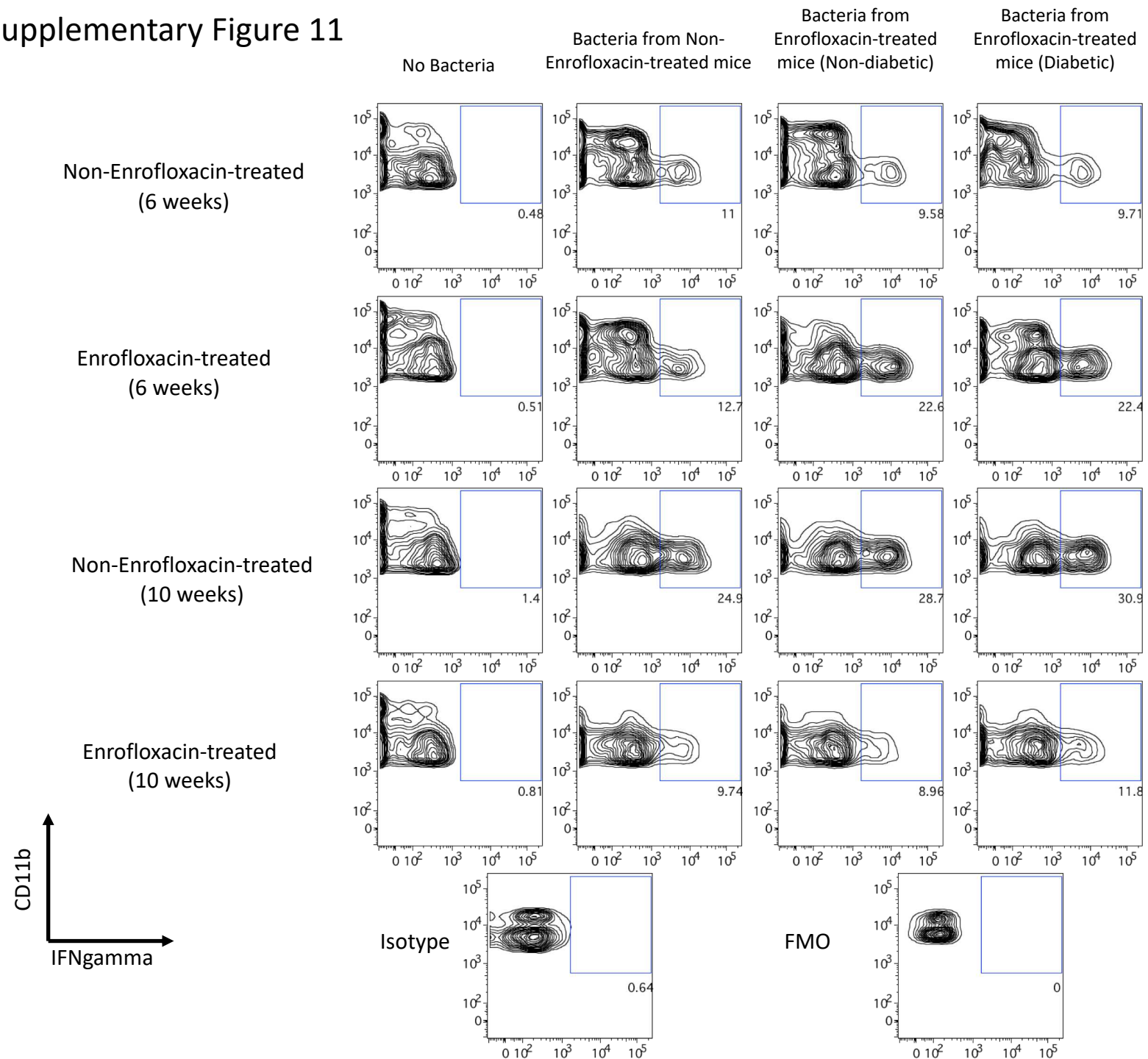

Supplementary Figure 12

Pearson et al

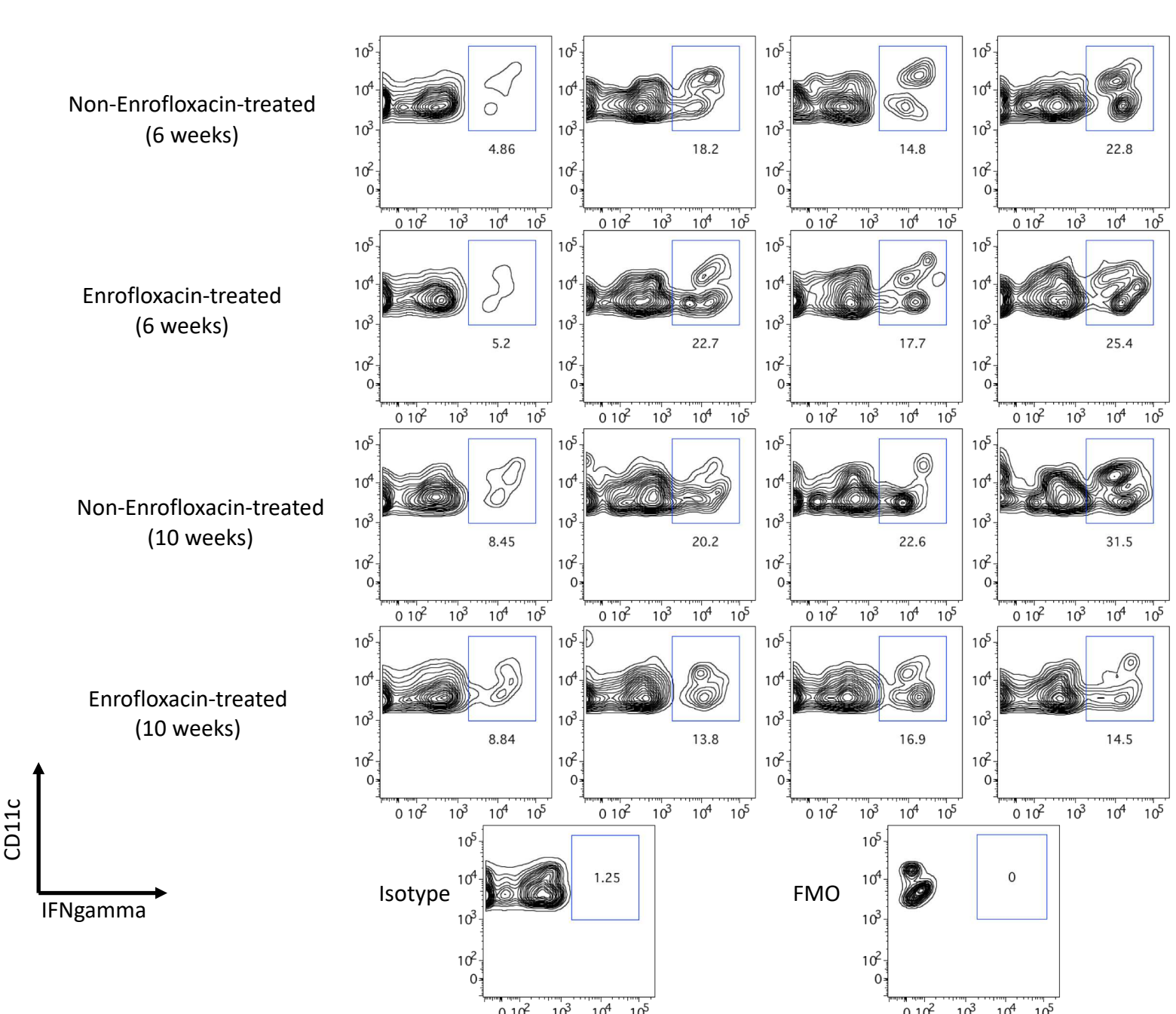

Supplementary Figure 13

Pearson et al

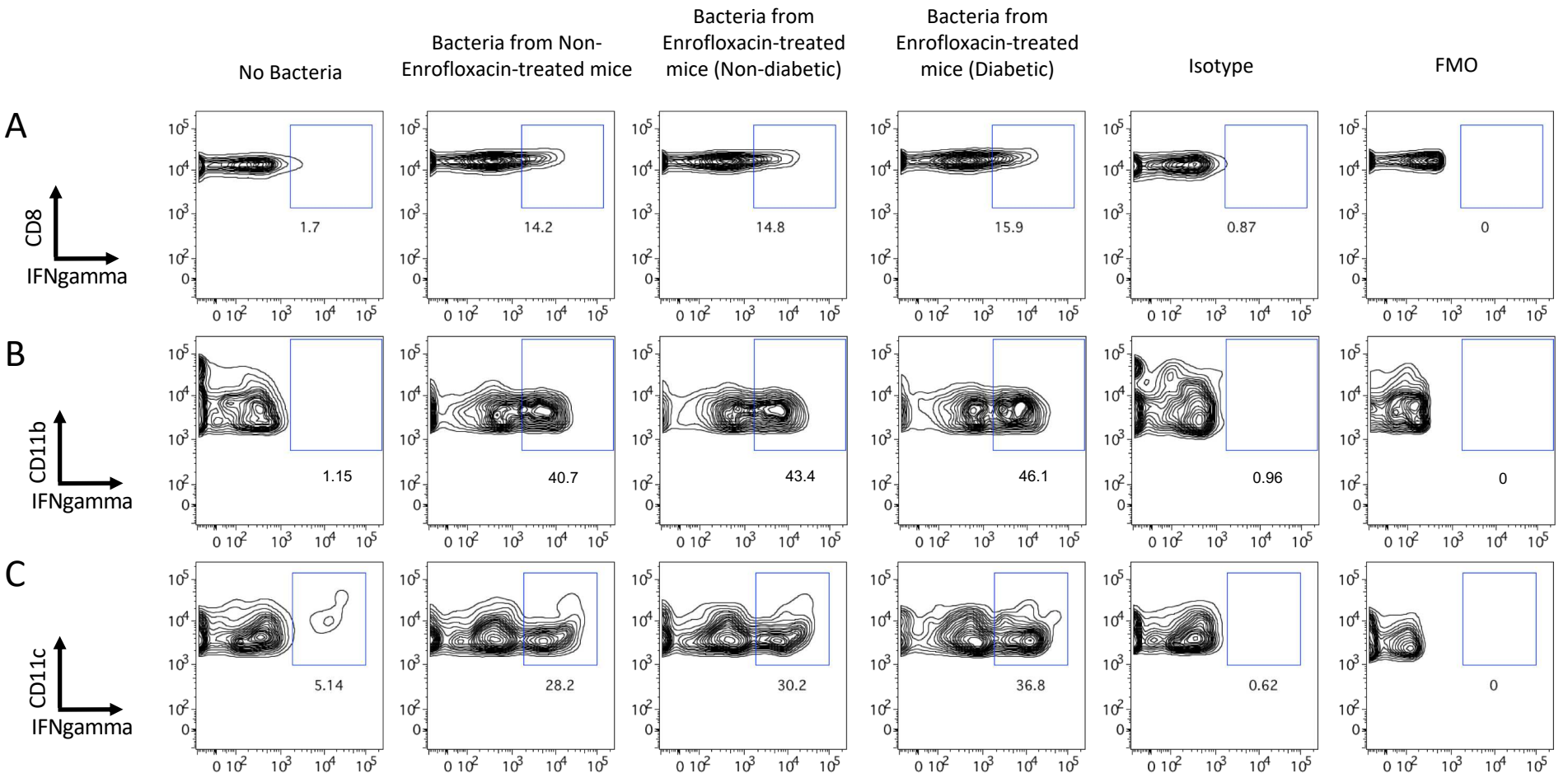

A

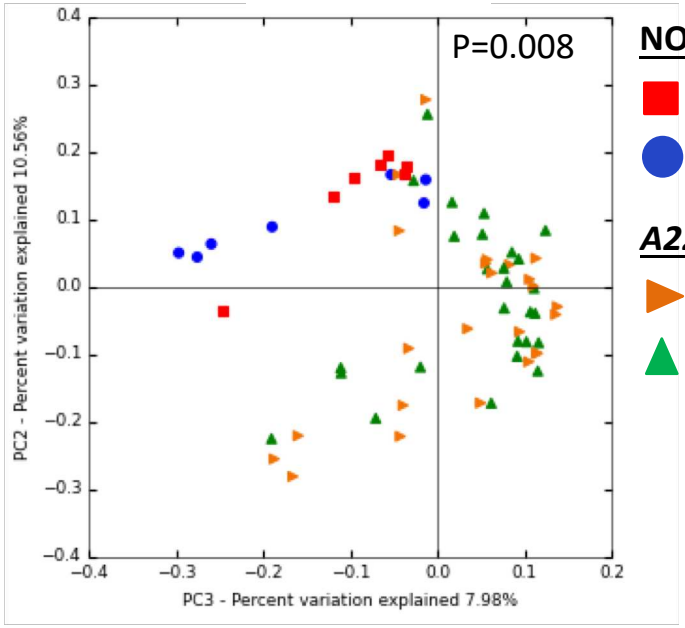

NOD

No Enrofloxacin

Enrofloxacin-treated

***A22Cα$^{-/-}$PI2$^{-/-}$*NOD**

No Enrofloxacin

Enrofloxacin-treated

Supplementary Figure 15

Pearson et al

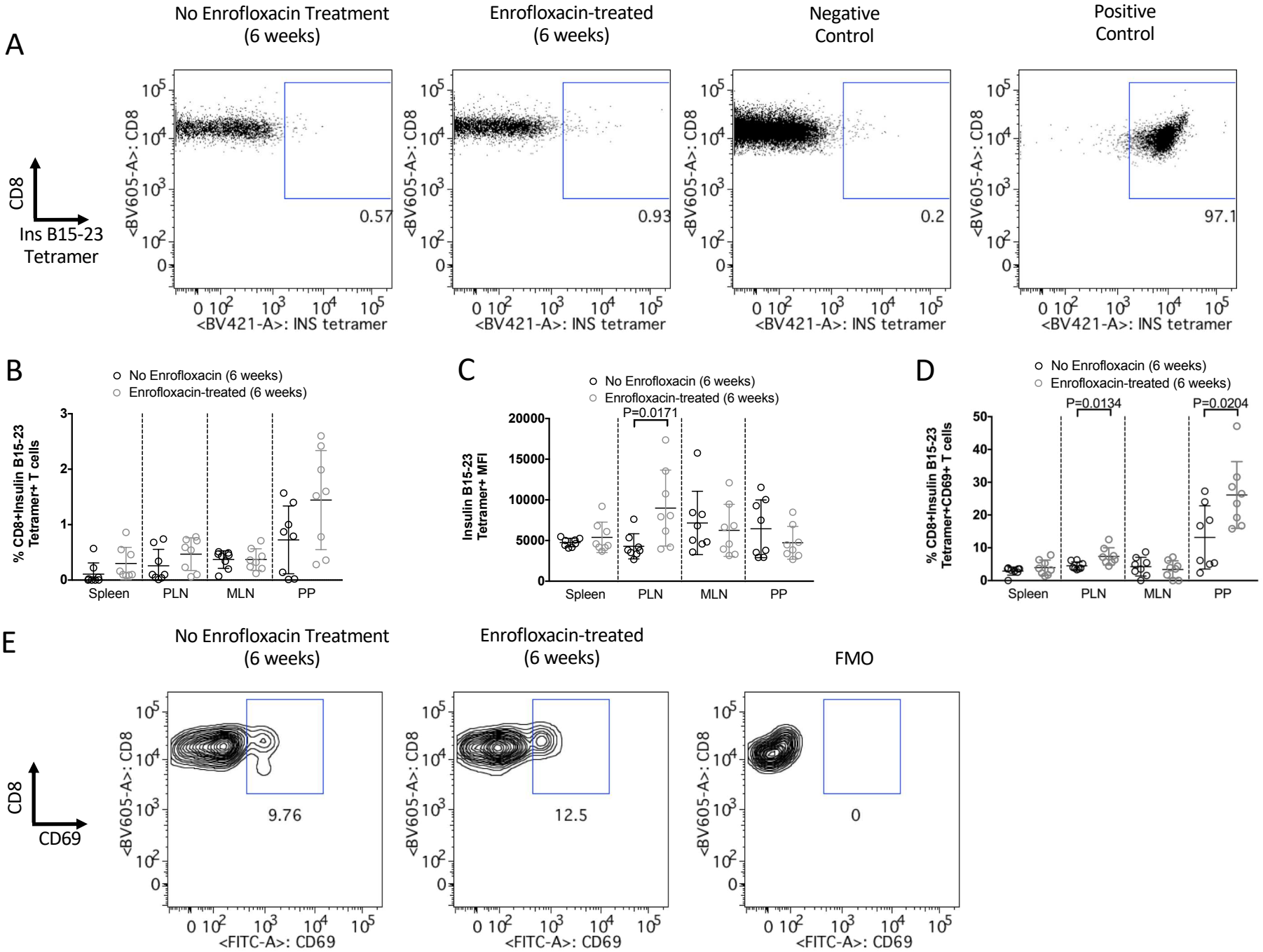

Supplementary Figure 16

Pearson et al

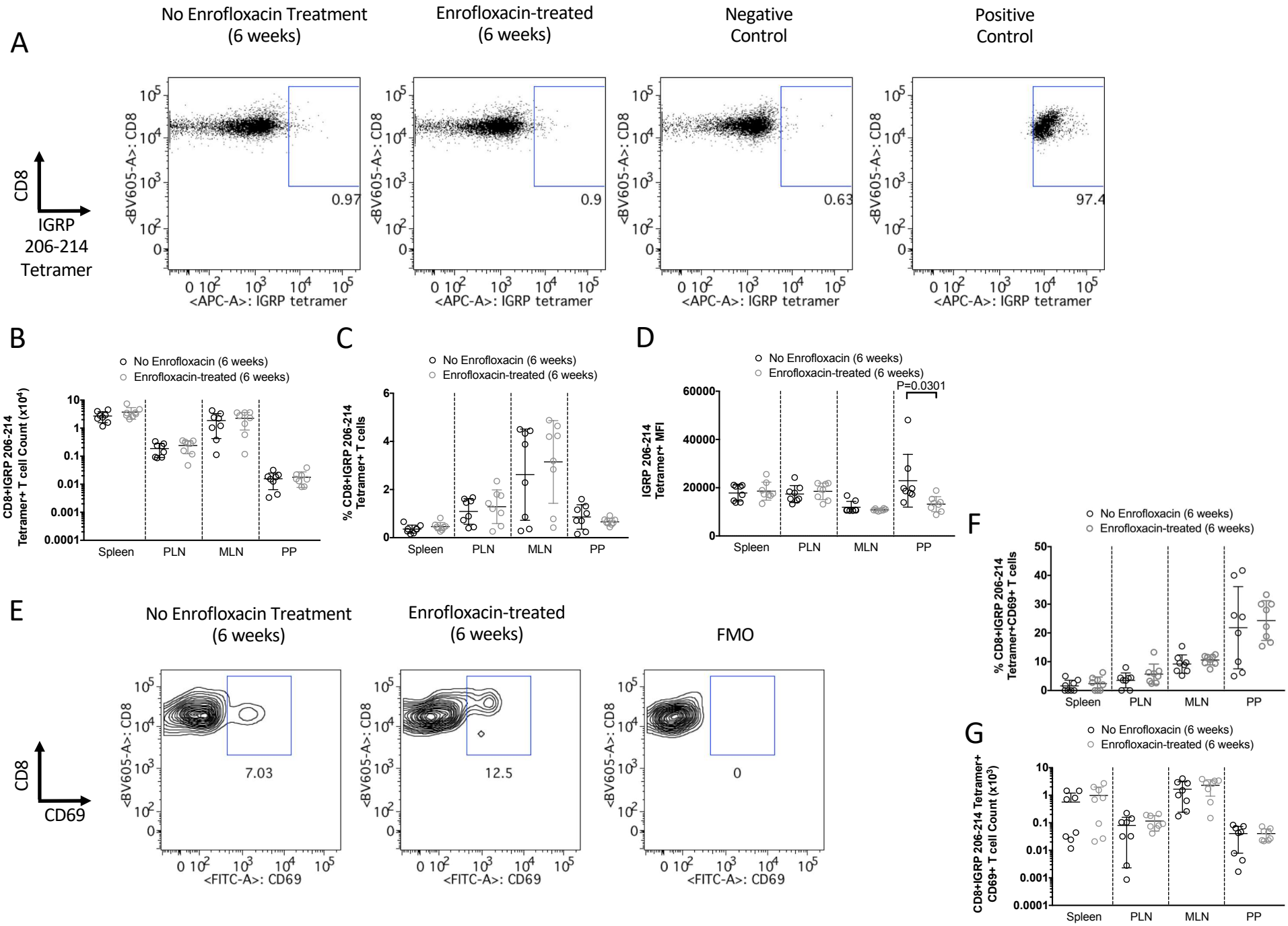

Supplementary Figure 17

Pearson et al